Jiang *et al. Energy Mater* 2022;2:200038
**DOI:** 10.20517/energymater.2022.52

**Energy Materials**

**Review**

**Open Access**

# Anodization fabrication techniques and energy-related applications for nanostructured anodic films on transition metals

**Longfei Jiang[1], Pengze Li[1], Shiyi Wang[1], Rui Liu[1], Xufei Zhu[1], Ye Song[1,*], Teunis van Ree[2]**

[1]Key Laboratory of Soft Chemistry and Functional Materials of Education Ministry, Nanjing University of Science and Technology, Nanjing 210094, Jiangsu, China.
[2]Department of Chemistry, University of Venda, Thohoyandou 0950, South Africa.

[*]**Correspondence to:** Prof. Ye Song, School of Chemistry and Chemical Engineering, Nanjing University of Science and Technology, No. 200 Xiaolingwei Street, Nanjing 210094, Jiangsu, China. E-mail: songye@njust.edu.cn

**How to cite this article:** Jiang L, Li P, Wang S, Liu R, Zhu X, Song Y, van Ree T. Anodization fabrication techniques and energy-related applications for nanostructured anodic films on transition metals. *Energy Mater* 2022;2:200038. https://dx.doi.org/10.20517/energymater.2022.52

**Received:** 7 Sep 2022 **First Decision:** 6 Oct 2022 **Revised:** 21 Oct 2022 **Accepted:** 1 Nov 2022 **Published:** 14 Nov 2022

**Academic Editor:** Yuping Wu **Copy Editor:** Fangling Lan **Production Editor:** Fangling Lan

## Abstract

Nanostructured anodic films on transition metals prepared using the electrochemical anodization method have recently attracted particular attention owing to their extraordinary properties and potential use in a variety of applications. Herein, we provide a thorough review of the anodization fabrication of anodic films with different nanostructures, including nanopores, nanotubes, nanoflowers, nanoneedles and nanowires on transition metals, focusing on the growth processes of nanostructured anodic films on three representative transition metals, namely, iron, copper and zinc. Specific consideration is given to the anodization behavior and formed film nanostructures of these transition metals. We conclude that electrolyte composition plays a key role in influencing the final morphologies of anodic films. Fluoride-containing solutions represent universal electrolytes for forming nanostructured anodic films on transition metals. The main applications of the resulting nanostructured anodic films, especially in energy-related fields, such as photoelectrochemical water splitting and supercapacitors, are also presented and discussed. Finally, we indicate the main challenges associated with the fabrication of anodic films with highly ordered nanostructures and the potential future directions of this field are indicated.

**Keywords:** Anodization, transition metals, anodic films, nanostructures, applications

## INTRODUCTION

Transition metal oxides, especially nanostructured oxides, are well known as a fascinating class of materials because of their rich and unique physical, chemical and mechanical properties. Among the various methods used for the fabrication of nanostructured transition metal oxides, the electrochemical anodization technique has gained increasing attention due to its simplicity, reproducibility and low-cost processing. To date, the most successful efforts to produce nanostructured anodic films have been for the anodization of aluminum (Al). Porous anodic aluminum oxide (AAO) films can be grown on Al by anodizing Al metal in acidic electrolytes (e.g., sulfuric ($H_2SO_4$), oxalic and phosphoric ($H_3PO_4$) acids)[1]. These porous AAO films consist of a thin barrier oxide layer over the Al surface and an overlying porous oxide layer, where each cylindrical nanopore and its surrounding oxide region form a hexagonal cell orientated perpendicular to the Al surface. These highly ordered AAO films with a honeycomb-like cell arrangement can be achieved under specific anodization conditions[2-5]. Consequently, by taking advantage of their highly ordered nanopores, porous AAO films have been widely utilized as templates for the fabrication of functional nanostructures.

Following the success of the anodization route in making highly ordered AAO films, this anodization method for the production of nanostructures has been applied to other metals, including transition metals. In 2001, the Grimes group first reported the formation of uniform $TiO_2$ nanotube arrays by the anodization of titanium (Ti) in a dilute aqueous hydrofluoric acid (HF) electrolyte[6]. However, the obtained nanotube arrays exhibited relatively poor ordering of the nanotube arrangement and the maximum nanotube lengths were limited to ~500 nm. Later, the Schmuki group demonstrated the growth of longer and ordered $TiO_2$ nanotube arrays during the anodization of Ti in fluoride-containing ethylene glycol (EG) electrolytes[7-9]. Since then, there have been considerable advances in the anodization of Ti. The morphological control of anodic $TiO_2$ nanotubes has become of significant interest and a large number of studies in this field have been published[10]. Anodization is currently a well-established technique for the fabrication of $TiO_2$ nanotube arrays.

Motivated by the success of anodization in the development of $TiO_2$ nanotubes, a variety of other transition metals have also been explored for the fabrication of nanostructured anodic oxides. Fluoride-based organic electrolytes were found to provide a very versatile approach to form nanostructured anodic films on other transition metal surfaces. For instance, a highly ordered nanoporous vanadium oxide film with a thickness of 13 μm and a pore diameter of ~15 nm was obtained by the anodization of vanadium foil at 120 V for 2 h in an EG electrolyte containing 0.2 mol $L^{-1}$ HF and 300 ppm Ti. A nanotubular structure was formed by increasing the anodization time to 24 h[11]. Furthermore, self-ordered nanoporous vanadium oxide films can be grown in EG-containing aqueous $NH_4BF_4$ and $NaBF_4$ solutions[11-13]. Similarly, other transition metal oxides (e.g., cobalt[14,15], molybdenum[16-19] and tungsten[20]) with ordered nanopores and other morphologies were obtained by anodization in fluoride-based electrolytes.

Over the past two decades, there has been growing interest in the anodization of various transition metals. Anodic films on a variety of transition metals with different nanostructures have been developed, leading to the discovery of many exciting properties and applications for transition metal oxides. The main goal of this review is to fully understand the state-of-the-art regarding nanostructured anodic films on transition metals by outlining the anodization behavior of several transition metals. Since a number of excellent reviews on anodic $TiO_2$ nanotubes have been published[10,21-23], the transition metals discussed here do not include Ti. Considering the tremendous amount of research involving the electrochemical anodization of transition metals, it is not possible to review all examples in the literature. Therefore, we select iron (Fe), copper (Cu) and zinc (Zn) as representative transition metals, because they are three of the most widely studied transition metals in this field in addition to Ti. This review article provides a comprehensive outlook of

these three transition metals. Particular attention is given to their anodization behavior and resultant nanostructures. The main applications of the corresponding nanostructured anodic films on transition metals, especially in energy-related fields, such as photoelectrochemical (PEC) water splitting and supercapacitors, are presented and discussed. Finally, the potential future directions and challenges for the anodization of transition metals are considered.

## IRON

Benefitting from the success of the electrochemical anodization route for making ordered $TiO_2$ nanotube arrays[21], the Grimes group was the first to report a successful attempt to synthesize nanostructured iron oxides by anodization in 2006[24]. They obtained iron(III) oxide with nanoporous structures by the anodization of Fe foil in glycerol electrolytes containing HF, $NH_4F$ and $HNO_3$. Since then, there has been a surge of interest regarding the fabrication of nanostructured iron oxides by anodization.

### Nanoporous and nanotubular arrays

To avoid local acidification at the oxide-electrolyte interface, the Grimes group chose glycerol as the electrolytic medium[24]. They prepared nanoporous anodic films on Fe foils by the potentiostatic anodization of Fe in glycerol containing HF, $NH_4F$ and $HNO_3$ at 10 °C. Unlike the anodization currents observed for the anodization of Al[1] or Ti[10], the anodization current for Fe decreased monotonically with time during anodization, whereas the typical current-time behavior for the anodization of Al or Ti is characterized by an increase in the current amplitude after an initial rapid current drop. The Grimes group explored the influence of anodization bath temperature, electrolyte composition and applied voltage on the pore size of the as-anodized nanoporous structures. For example, nanoporous films with a barrier layer thickness of ~800 nm could be formed by anodization at 90 V for 2 h at 10 °C. Nevertheless, the as-anodized nanoporous films obtained in the electrolyte containing HF, $NH_4F$ and $HNO_3$ in glycerol had relatively disordered porous structures with a typical pore depth of only ~500 nm. Interestingly, the authors obtained a highly ordered nanoporous structure by anodization at a constant voltage of 40 V at 10 °C when using 0.3 wt.% $NH_4F$ in EG as an electrolyte. The cylindrical nanochannels of the obtained nanoporous anodic films on Fe substrates were very similar to those found in porous AAO[1,25,26].

Following the pioneering work of Grimes and coworkers, high-aspect-ratio and relatively ordered nanoporous anodic films were later developed. The Schmuki group utilized $NH_4F$/EG-based electrolytes similar to those used in the fabrication of $TiO_2$ nanotube arrays to prepare relatively ordered nanoporous anodic films on Fe at 20 °C[27]. The resulting porous layer had a significantly increased thickness (up to ~13 μm) compared with those obtained in the glycerol electrolyte. The resulting porous layer was confirmed to be essentially amorphous and the nanopores were most probably comprised of a relatively compact inner oxide shell and $FeF_2$-rich outer shell[27]. Using Mössbauer spectroscopy at room to cryogenic temperatures, Jagminas *et al.* demonstrated that their as-prepared iron anodic films mainly consisted of lepidocrocite (γ-FeOOH) with some $Fe(OH)_2$ and/or $FeF_2 \cdot 4H_2O$[28]. In addition, Habazaki *et al.* also obtained porous anodic films on Fe in the same EG electrolytes containing $NH_4F$ and $H_2O$ by galvanostatic anodization instead of the commonly used potentiostatic anodization[29-31]. Their studies showed that the porous anodic films could always be formed provided that anodization was performed galvanostatically at a constant current density of less than 10 mA $cm^{-2}$ at temperatures below 30 °C.

Schmuki and coworkers observed an interesting temperature effect, where anodization at higher temperatures could induce a morphological change from the porous layer to nanotube arrays under otherwise identical conditions[27]. Later, LaTempa *et al.* reported the formation of anodic oxide nanotube arrays by the potentiostatic anodization of Fe in $NH_4F$/EG-based electrolytes at higher temperatures[32]. The

authors were able to produce iron oxide nanotube arrays using EG electrolytes containing 0.2-0.5 wt.% $NH_4F$ and 2%-4% $H_2O$ over a voltage range of 30-60 V by changing the electrolyte temperature. For instance, when the anodization of Fe foil was conducted at 50 V for 180 s in an EG electrolyte containing 0.3 wt.% $NH_4F$ and 3% $H_2O$ at a starting bath temperature of 60 °C, vertically oriented nanotube arrays with an average pore diameter of 55 nm and length exceeding 3 μm were obtained. It was suggested that the formation of nanotube arrays strongly depended on the electrolyte bath temperature and $NH_4F$ concentration. However, at room temperature, Rangaraju *et al.* were also able to prepare nanotubular oxide films by anodization in a similar EG solution at 50 V for 15 min[33,34]. The obtained nanotubes with a length of ~1.5 μm had an inner diameter of 54-100 nm and a wall thickness of 12-22 nm. Later work suggested that, for the anodization of Fe at room temperature for 30 min, increasing the water content or anodization voltage led to the transformation of nanotubes to nanoparticles or nanowires, respectively[35].

Consequently, the formation of nanotubes was believed to be associated with the extended anodization times in addition to the electrolyte temperature. In reality, the stirring of the electrolyte[28,36], the applied magnetic field[36] and the rotation speed of the Fe electrode[37,38] during anodization can also influence the nanostructures of anodic films on a Fe substrate. Of course, the purity of the Fe substrate also plays an important role in determining the formation of iron oxide nanostructures. Lee *et al.* investigated the anodization behavior of two Fe substrates with purities of 99.5% and 99.99% at room temperature, at 60 °C and under ultrasonication-assisted conditions, respectively[39]. They found that there was a notable difference in the thickness of the obtained anodic films for the two Fe substrates regardless of which anodization conditions were used. Although there was no significant difference in the top morphologies for both substrates, the anodic films grown on the 99.99% purity Fe substrate were typically twice as thick as those grown on the 99.5% purity substrate for the same anodization time[39].

Some fabrication techniques available for anodic $TiO_2$ nanotubes and porous AAO can also be used in the electrochemical anodization of Fe. For example, Fe anodization experiments were carried out using ultrasonic waves[39-42]. Nanotubular array films on Fe foils could be grown by ultrasound-assisted anodization due to the introduction of additional energy[39-41]. To prepare porous anodic iron oxide films with more ordered nanopores, the so-called "two-step anodization" process was also utilized in the anodization of Fe[43-47]. In this process, an anodic film grown on the Fe foil by the first anodization process was removed to obtain a Fe surface textured with arrays of concave features. After the second anodization, a self-ordered porous anodic film was formed, apparently because these concave features guide the growth of nanopores. In addition to the usual potentiostatic and galvanostatic anodization, sinusoidally modulated current waveforms were also employed in the anodization of Fe[48]. Interestingly, periodically structured porous anodic films were obtained by applying a sine-wave current or a voltage pulse to the Fe electrode[49]. By changing the periodicity of the sine-wave current, the structural periodicity of the obtained anodic films and the film color could be tuned[48]. The reported anodization conditions for the fabrication of nanoporous or nanotubular iron oxide arrays are listed in Table 1, along with their morphological parameters.

### Formation mechanism

For the potentiostatic anodization of Fe, the current-time transients during anodization typically display three different stages, as shown in Figure 1A[50], which are very similar to those observed for the anodization of Al or Ti[1,10,32,34,40,45,47,50,52]. Therefore, it is presumed that the nanostructured anodic films on Fe were formed in a manner analogous to the growth of porous AAO or $TiO_2$ nanotube arrays. Following the suggested mechanism for the formation of anodic $TiO_2$ nanotubes, some authors proposed the possible formation mechanism of iron oxide nanopores or nanotubes formed by anodization in $NH_4F$/EG-based electrolytes[47,50,59]. It is generally believed that the formation of iron oxide nanopores or nanotubes involves two electrochemical/chemical processes, namely, the field-assisted oxidation of Fe metal either to form iron

**Table 1. Anodization conditions and morphological parameters of samples anodized in various electrolyte systems**

| Solvent | Electrolyte (wt.%) | Water content | Anodization voltage/current | Anodization duration | Bath emperature (°C) | Pore/Tube diameter (nm) | Nano structure | Degree of ordering | Pore/Tube length (μm) | Refs. |
|---|---|---|---|---|---|---|---|---|---|---|
| Glycerol | 0.5 wt.% $NH_4F$ + 1wt.% HF + 0.2 wt.% $HNO_3$ | 0 | 40-90 V | 2 h | 10 | 50-250 | nanopore | poor | 0.3-0.6 | [24] |
| EG | 0.3 wt.% $NH_4F$ | 0 | 40 V | 15 min | 10 | 30 | nanopore | good | 2.5 | [24] |
| EG | 0.1 M $NH_4F$ | 1 M | 10-100 V | 1 h | 20 | 40-110 | nanopore | good | 1-13 | [27] |
| EG | 0.1-0.4 wt.% $NH_4F$ | 1.5-3.5 vol.% | 30-100 V | 2.5 h | 10-20 | 92 | nanopore | fair | 10 | [28] |
| EG | 0.1 M $NH_4F$ | 0.1-1.5 M | 5 mA $cm^{-2}$ | 900 s | 20 | 8-50 | nanopore | poor | 0.7 | [29] |
| EG | 0.1 M $NH_4F$ | 0.3-3.5 M | 1-10 mA $cm^{-2}$ | 0.5-2 h | 10-30 | 20-125 | nanopore | fair | 7 | [30] |
| EG | 0.2-0.5 wt.% $NH_4F$ | 2%-4% | 30-60 V | 30-180 s | 60-75 | 35-65 | nanotube | good | 4 | [32] |
| EG | 0.1 M $NH_4F$ | 3 vol.% | 50 V | 15 min | RT | 54-100 | nanotube | fair | 1.5 | [33, 34] |
| EG | 0.5 wt.% $NH_4F$ | 3 vol.% | 50 V | 13 min | using ultrasonic waves | 50-60 | nanotube | fair | 3.77 | [40] |
| EG | 0.5 wt.% $NH_4F$ | 3 vol.% | - | - | using ultrasonic waves | 40 | nanotube | fair | 2 | [41] |
| EG | 0.3 wt.% $NH_4F$ | 2 vol.% | 50 V (two-step) | 5 min | RT | 40 | nanopore | fair | 2 | [43] |
| EG | 0.1 M $NH_4F$ | 1 M | 40 V (two-step) | 1 h | 20 | 60-100 | nanopore | good | 5 | [45, 46] |
| EG | 0.1 M $NH_4F$ | 3 vol.% | 50 V (two-step) | 15 min | 30 | 50 | nanopore | fair | 0.6 | [47] |
| EG | 0.1 M $NH_4F$ | 1.5 vol.% | sine-wave current | 405-645 s | 60 | 30-120 | nanopores with structural periodicities | good | 3 | [48] |
| EG | 0.5 wt.% $NH_4F$ | 3 wt.% | 50 V | 5 min | 60 | 120 | nanotube | good | 3.6 | [50] |
| EG | 0.5 wt.% $NH_4F$ | 3 vol.% | 50 V | 5 min | 60 | 100 | nanotube | good | 3 | [51] |
| EG | 0.1 M $NH_4F$ | 1 M | 40 V | 1 h | 25 | 50-70 | nanotube | fair | - | [52] |
| EG | 0.35 wt.% $NH_4F$ | 2.7 wt.% | 50 V | 15 min | RT | 30 | nanopore | fair | 1.8 | [53] |
| EG | 0.5 wt.% $NH_4F$ | 1.3 M | 60 V | 90-150 s | - | 47-51 | nanopore | fair | 1.4-1.8 | [54] |
| EG | 0.8 wt.% $NH_4F$ | 2 M | 60 V | 90-150 s | - | 62-79 | nanotube | fair | 2.2-2.7 | [54] |
| EG | 0.35 wt.% $NH_4F$ | 3 vol.% | 50 V | 10-20 min | 20-50 | 50 | nanotube | fair | - | [55] |
| EG | 0.2 M $NH_4F$ | 3 vol.% | 50 V | 5 min | 20 | - | nanopore | fair | 1 | [56] |
| EG | 0.7 wt.% $NH_4F$ | 2 vol.% | 40 V | 15 min | - | 40 | nanopore | fair | - | [57] |
| EG | 0.1 M $NH_4F$ | 3 vol.% | 50 V | 15 min | 25 (electrode rotation) | 75 | nanotube | fair | 0.8-0.95 | [58] |
| EG | 0.2 M $NH_4F$ | 2 M | 50 V | 5 min | 23 (stirring) | 40 | nanopore | fair | 1.5 | [59] |
| EG | 0.2 M $NH_4F$ | 0.5 M | 20-60 V | 1 h | 20 (not stirring) | 60-89 | nanopore | fair | 1.98-3.61 | [60] |

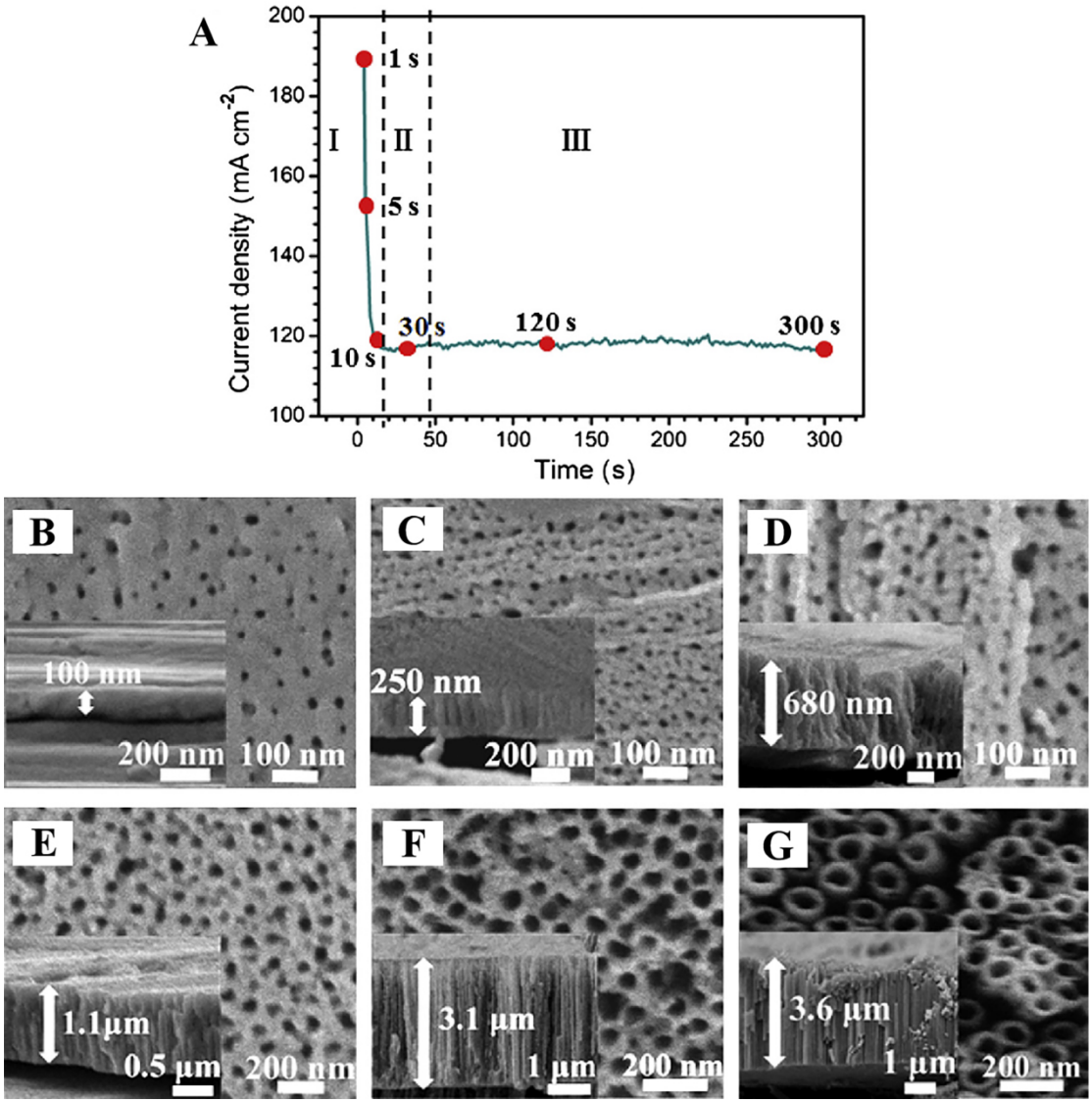


**Figure 1.** (A) Current density transient during the anodization of Fe foil at 50 V in EG + 0.5 wt.% $NH_4F$ + 3.0 wt.% water for 300 s at 60 °C. (B-G) FESEM images of anodic iron oxide films after 1, 5, 10, 30, 120 and 300 s, respectively. Insets show the corresponding cross-sectional image at each stage[50]. Reproduced from Ref.[50] with permission from Elsevier.

oxides or Fe ions dissolved in the electrolyte and the chemical dissolution of iron oxides owing to etching by fluoride ions. A delicate equilibrium between the formation and dissolution of iron oxide films results in nanopore or nanotube formation.

The current-time behavior shown in Figure 1A can be understood in terms of the above-described model. In $NH_4F$/EG-based electrolytes containing water, an initial oxide layer is first formed on the Fe substrate at the metal-electrolyte interface according to Equation 1 when an anodization voltage is applied. This process corresponds to a rapid decrease in current density, as shown in Figure 1A at the initial stage (stage I), as a result of the fast formation of the insulating iron oxide layer. Subsequently, localized chemical etching of the iron oxide can take place to form some disordered small pits in the oxide layer due to the formation of soluble fluoro complexes, according to Equation 2. In this stage (stage II, Figure 1A), a slight rise in current occurs since these small pits increase the surface area of the Fe anode. At the bottom of the small pits, the

electric field strength is higher than at other locations due to the relatively thin barrier layer, thereby giving rise to the emergence and/or growth of pores. As anodization proceeds, the pores tend to share the anodization current equally, leading to the formation of an ordered nanoporous film. In this stage (stage III, Figure 1A), the anodization current stays almost constant, implying the establishment of an equilibrium between the formation and dissolution of iron oxides. With a further increase in the anodization time, transformation of the ordered nanoporous structures into nanotube arrays eventually occurs, largely due to the selective dissolution of the Fe fluoride-rich layer at the cell boundaries. Xie *et al.* investigated systematically the effects of anodization conditions on the morphology and growth behavior of anodic iron oxide films and presented the morphological evolution of anodic films during anodization, as depicted in Figure 1B-G[50].

$$2Fe + 3H_2O \rightarrow Fe_2O_3 \text{ (anodic)} + 3H_2\uparrow \text{ (cathodic)} \quad (1)$$

$$Fe_2O_3 + 12F^- + 6H^+ \rightarrow 2[FeF_6]^{3-} + 3H_2O \quad (2)$$

Recently, some researchers[59,61] have argued that the formation of nanoporous anodic films on Fe can also be explained in terms of the electronic current and oxygen bubble model suggested by our group in the case of porous AAO or anodic $TiO_2$ nanotubes[62-66]. This model emphasizes that the formation of nanopores is closely related to oxygen gas generation during anodization. The anodization currents (consisting of ionic and electronic currents) are not all consumed to form the oxide. During anodization, the ionic currents originating from the migration of oxygen/metal ions lead to oxide growth, while the electronic currents give rise to the evolution of oxygen gas at the bottoms of the pores. Furthermore, the generation of bubbles all over the Fe anode surface could be observed clearly during the Fe anodization. It was suggested that nanopores in the anodic films on Fe were generated by the flow of the material in the barrier layer from the pore bases towards the pore walls around the gas bubble under the pressure of bubbles and growth stresses.

### Other nanostructures

In addition to the most commonly found nanoporous and nanotubular structures, the anodization of Fe in the $NH_4F$-$H_2O$-EG electrolyte system can also result in anodic films with other morphologies[67,68]. Kang *et al.* synthesized vertically aligned iron oxide nanoflakes on the surface of a Fe foam by anodization at 80 V for 5 min at 25 °C with the assistance of ultrasonication in an EG electrolyte containing 0.25 wt.% $NH_4F$ and 2 vol.% $H_2O$[67]. The authors reported that electrolyte composition plays a critical role in influencing the final morphologies of anodic films. To demonstrate this concept, they conducted the anodization of Fe foil in four EG electrolytes with different compositions. An interesting phenomenon observed in their study was that, as shown in Figure 2, as the concentrations of $NH_4F$ and $H_2O$ increased, anodic iron oxide films with different nanostructures ranging from nanoflakes to nanotubes were obtained[67]. Later, Ali *et al.* reported the synthesis of a three-dimensional nanoflower-like (composed of nanoflakes) hierarchical morphology of iron alkoxide by anodization. Anodization was performed at 50 V at room temperature for 1 h using an EG electrolyte containing 0.5 wt.% $NH_4F$ and 0.2 wt.% $H_2O$[68]. Compared to the frequently observed nanoporous and nanotubular structures, the only major difference in anodization conditions was the utilization of an EG electrolyte with a very low water content in their nanoflower fabrication. When the EG in this electrolyte was changed to glycerol, the anodization of Fe foil under identical conditions was found to induce the formation of nanotubes rather than nanoflowers. Therefore, the authors suggested that EG plays a pivotal role in obtaining the nanoflower-like morphology[68].

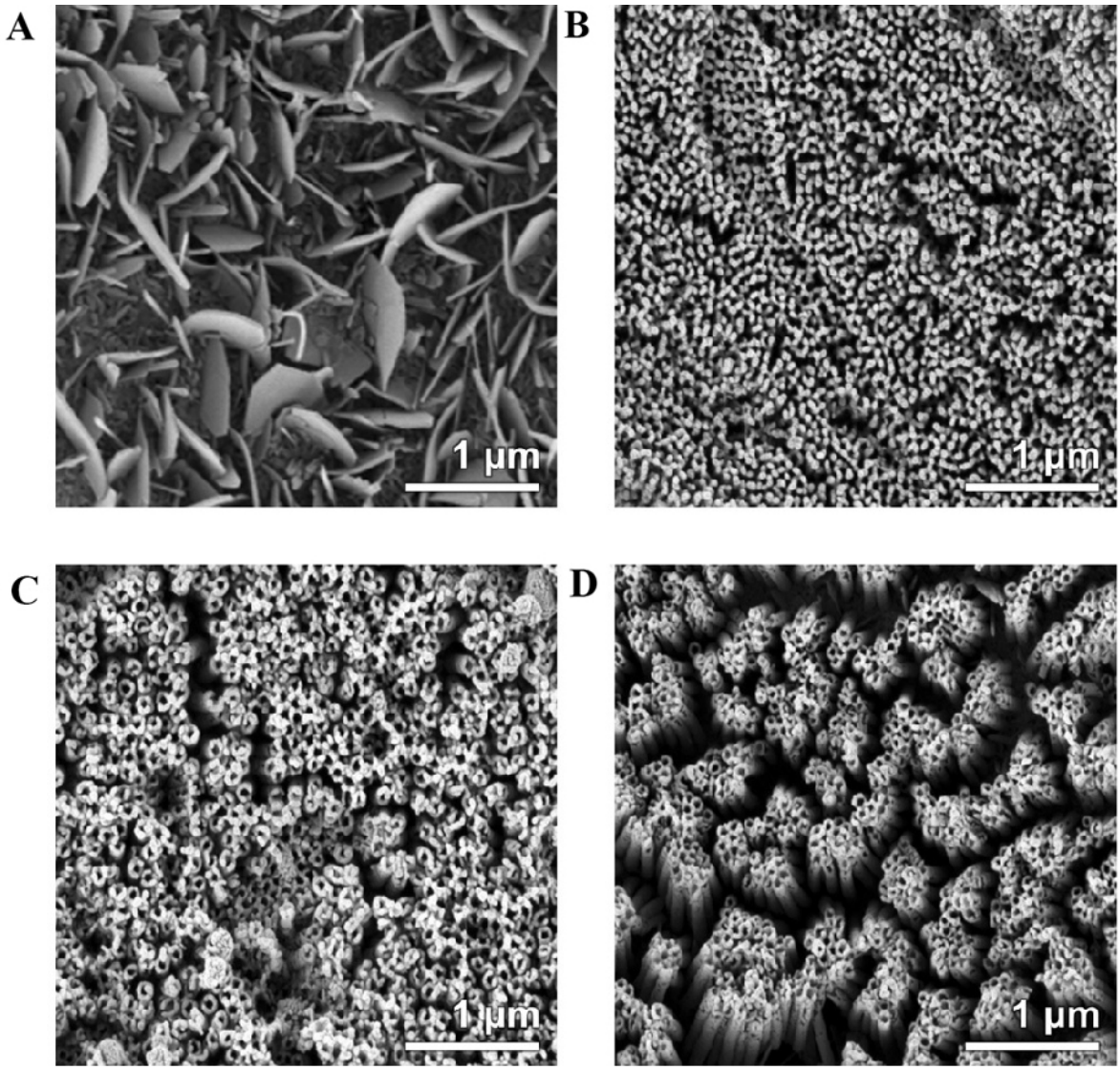


**Figure 2.** SEM images of iron oxide nanostructures prepared by anodization of Fe foil at 50 V for 1 h using EG electrolytes of various compositions: (A) 0.125 wt.% $NH_4F$ and 1.0 vol.% $H_2O$; (B) 0.250 wt.% $NH_4F$ and 2.0 vol.% $H_2O$; (C) 0.500 wt.% $NH_4F$ and 3.0 vol.% $H_2O$; (D) 1.000 wt.% $NH_4F$ and 4.0 vol.% $H_2O$[67]. Reproduced from Ref.[67] with permission from Wiley.

Several investigations have sought to generate other nanostructured anodic films on Fe substrates in fluoride-free electrolyte systems[69-71]. Sagu *et al.* employed a 10 mol $L^{-1}$ aqueous NaOH solution as the electrolyte for the anodization of steel[69]. The surface layer of the anodized steel was confirmed to be $Fe_2O_3$ with a highly porous sponge-like structure. Recently, our group[70,71] carried out the anodization of Fe using an aqueous oxalic acid solution. Interestingly, the anodic film grown on Fe exhibited a rod-like morphology, with the rods having relatively regular hexahedral shapes with feature sizes of 250-700 nm. FTIR and XRD analyzes showed that the as-anodized films essentially consisted of amorphous ferrous oxalate[70].

Finally, it is worth emphasizing that, unlike anodic $TiO_2$ nanotubes, the nanostructures (nanopores and nanotubes) of as-anodized iron oxide films generally undergo a significant change after thermal annealing due to an amorphous to crystalline transition[31,36,38,46,50,53,55,56,68,72]. To inhibit the morphological changes of the anodic iron oxide films as a result of the agglomeration of the hematite particles during thermal annealing,

Jun *et al.* specifically devised a 10 nm-thick alumina layer deposited on the surface of nanopores as a shielding layer to maintain the vertically ordered nanoporous structure of the hematite[44].

## Applications

Iron oxides, like FeO, $Fe_2O_3$ and $Fe_3O_4$, have attracted intense research interest for various applications, including photocatalysis[49], PEC water splitting[38,39,44,67], lithium-ion batteries[45,46], supercapacitors[51] and biomaterials[54,73], because of their unique electrochemical/PEC properties, crystallographic polymorphism, earth abundance, eco-friendliness and low cost. Here, we focus on their applications in the PEC fields and electrochemical energy storage devices.

### *PEC applications*

Since α-$Fe_2O_3$ (hematite) has a band gap of 2.0-2.2 eV, which allows the harvesting of nearly 40% of the solar spectrum with a maximum theoretical photoconversion efficiency of 12.9%[74,75], it has increasingly gained attention as a promising material for PEC applications. In fact, investigations of nanoporous iron(III) oxide synthesized by anodization, first reported by the Grimes group, have been mainly focused on PEC applications[24]. They found that annealed nanoporous $Fe_2O_3$ films exhibited a net photocurrent density of 0.51 mA $cm^{-2}$ at 0.6 V *vs.* Ag/AgCl in an electrolyte containing 0.5 mol $L^{-1}$ $H_2O_2$ and 1 mol $L^{-1}$ NaOH under AM 1.5 simulated solar illumination. Since then, many studies have featured the PEC properties of nanostructured iron oxide films fabricated by anodization[31-35,37-40,42-44,49,52,53,56-58,67,72-75]. The Misra group demonstrated that a photoanode with a two-layer oxide structure comprising a top layer with a nanodendrite morphology and a bottom layer with a nanoporous morphology, obtained by the two-step anodization of Fe, exhibited noticeably improved photoactivity compared to that of a single layer nanotubular oxide[33,34]. Moreover, the authors produced ordered and ultrathin $Fe_2O_3$ nanotube arrays on Fe foil by an ultrasonic wave-assisted anodization process[40]. These ultrathin $Fe_2O_3$ nanotube arrays with a wall thickness of 5-7 nm and a length of 3-4 μm showed a photocurrent density of 1.41 mA $cm^{-2}$ at 0.5 V *vs.* Ag/AgCl with a maximum solar-to-hydrogen conversion efficiency of 0.84% under illumination with AM 1.5 solar light.

As mentioned above, the fabrication of vertically aligned iron oxide nanoflakes on the surface of a Fe foam using electrochemical anodization was reported by Kang *et al.* in 2017[67]. The anodized Fe foam photoanode was observed to have a photocurrent density exceeding 5 mA $cm^{-2}$ before reaching the dark current onset, which is the maximum value reported to date for PEC water splitting based on iron oxides. They attributed this excellent performance to the large surface area and low electrical resistance of the Fe foams[67]. More recently, Xue *et al.* reported the *in-situ* construction of a $Fe_2O_3/Fe_3O_4$ heterojunction by a facile two-step annealing process[76]. The as-anodized $Fe_2O_3$ nanotubes were annealed first at 400 °C in air and then at 500 °C in argon. Because the *in-situ* generated $Fe_2O_3/Fe_3O_4$ heterojunction facilitated the separation and transport of photogenerated carriers, the two-step annealed nanotubes exhibited a photocurrent of 2.5 mA $cm^{-2}$ at 1.6 V *vs.* a reversible hydrogen electrode (RHE), three times higher than that of pure $Fe_2O_3$ nanotubes.

It has been well-documented that the nanoscale morphology of iron oxides plays a crucial role in determining their PEC properties. For instance, Jun *et al.* fabricated highly ordered honeycomb hematite films by employing two-step anodization and a subsequent alumina shielding treatment before annealing[44]. The highly ordered nanoporous hematite films showed significantly higher photocurrent values compared to those with lower degrees of ordering. Mushove *et al.* found that the incident photon-to-current efficiency at 350 nm for the wave-like hematite nanotube arrays was about three times greater than that of single-layer nanotube arrays and about 12 times higher than that of multilayer nanotube arrays[49].

Furthermore, the PEC water splitting performance of the anodized iron oxides was found to be influenced by many factors, such as the purity of the Fe substrate[39], the annealing temperature[53], the anodization time[58], the rotation speed of the Fe substrate and electrolyte temperature during anodization[37,38] and the annealing atmosphere[56,72]. In addition to their very promising applications in PEC water splitting, anodic iron oxide nanotube arrays have also shown good photocatalytic performance in the degradation of methylene blue under visible light[42,52] and excellent oxygen reduction reaction catalytic activity[55]. In addition, Joseph *et al.* reported the synthesis of metal-doped iron oxide nanoporous structures achieved by an additional simple electrochemical process after Fe anodization[57,77]. The metal-doped iron oxide nanostructures exhibited enhanced photocatalytic activity.

*Electrochemical energy storage devices*

The wide variety of valence states and crystal structures of iron oxides makes it possible to use them as electrochemical energy storage devices, either as battery electrodes or supercapacitors[78,79]. The application of anodic $Fe_2O_3$ nanotubes in supercapacitors was first reported by Xie *et al.* in 2011[51]. They demonstrated that the resultant α-$Fe_2O_3$ nanotube arrays had a high specific capacitance of 138 $F \cdot g^{-1}$ at 1.3 $A \cdot g^{-1}$ and good rate capability (91 $F \cdot g^{-1}$ at 12.8 $A \cdot g^{-1}$). However, the cycling stability was found to be relatively poor, with a capacitance retention of only 88.9% after 500 cycles. More recently, Li *et al.* prepared a porous $Fe_3O_4$ film on Fe foil by anodization, followed by the electrodeposition of polyaniline onto the film by the electropolymerization of aniline[80]. The obtained $Fe_3O_4$/polyaniline hybrid electrode showed a specific capacitance of 47.11 $mF \cdot cm^{-2}$ at 1.3 $mA \cdot cm^{-2}$ and good cycling stability with a capacitance retention of more than 90% after 1500 cycles. Pervez *et al.* utilized $Fe_2O_3$ nanotube layers grown by anodization as a Li-ion battery anode[45,46]. They performed a comparative study of the electrochemical performance of crystalline and amorphous anodic iron oxide nanotube layers. The results indicated that the crystalline nanotubes exhibit greatly enhanced electrochemical properties, with a high specific capacity of 2.775 mAh $cm^{-2}$ at 0.1 mA $cm^{-2}$ and good rate capability (0.150 mAh $cm^{-2}$ at 0.8 mA $cm^{-2}$).

## COPPER

According to the Pourbaix diagram of Cu, its passivity at room temperature occurs in alkaline environments, meaning that alkaline electrolytes, such as NaOH, are typically used during the anodization of Cu. The investigation of the anodic behavior of Cu in alkaline solutions can be traced back to the 1940s[81]. The early studies focused on identifying the compositions of anodic films on Cu. The main products of Cu anodization in alkaline media were cuprous oxide $Cu_2O$, cupric oxide CuO, cupric hydroxide $Cu(OH)_2$ and water-soluble coordination anions like $Cu(OH)_4^{2-}$[81,84]. Later, the fabrication of nanostructured copper oxides/hydroxides attracted significant attention due to the advantageous properties of nanomaterials. The most straightforward route to nanostructures is template synthesis. For example, $Cu_2O$ nanowires were obtained by electrochemical deposition using polycarbonate or AAO templates[85,86]. However, unlike Al, Ti or Fe, it is difficult to obtain nanoporous or nanotubular oxides directly by the electrochemical anodization of Cu without any template. Fortunately, the anodization of Cu can also result in the formation of nanostructured copper oxides/hydroxides.

### Nanoneedles, nanowires and nanotubes

As early as 1976, Shoesmith *et al.* thoroughly investigated the anodic oxidation of Cu in a LiOH solution using potentiostatic, galvanostatic and voltammetric sweep techniques[87]. The main anodization product was demonstrated to be $Cu(OH)_2$, with the formation of CuO and $Cu_2O$ phases also possible in terms of the anodization conditions. The authors also discussed the nucleation and growth mechanism of $Cu(OH)_2$ films. Furthermore, the acicular morphology of the resultant films was first observed in their pioneering work[87]. In 2005, the Shi group utilized KOH-based electrolytes to form nanostructured anodic films on Cu

under galvanostatic conditions[88]. As shown in Figure 3, the typical anodic products exhibit a pine needle-like morphology, which was confirmed to be mainly $Cu(OH)_2$ with traces of $Cu_2O$. It is noteworthy that unlike the amorphous nature of the majority of anodic films on metals, the as-anodized products formed on Cu are crystalline. Figure 3 shows the morphological evolution of anodic films on Cu during anodization. After anodization for 1500 s, $Cu(OH)_2$ nanoneedles oriented roughly perpendicular to the Cu substrate covered the whole Cu surface [Figure 3D]. These nanoneedles had an average length of 15 μm with a typical diameter of 500-550 nm at their roots and 100-120 nm at their sharp tips. As the electrolyte temperature decreased, the number density of nanoneedles clearly increased, whereas their average length decreased correspondingly. This could be attributed to the easier nucleation of $Cu(OH)_2$ crystals at lower temperatures. Under otherwise identical conditions, scroll-like $Cu(OH)_2$ nanotubes were formed on Cu foil when the KOH concentration was increased to over 2.5 mol $L^{-1}$. Moreover, the current density also played an important role in governing the resulting anodic products. At a low current density of 0.5 mA $cm^{-2}$, black nanosheets or nanoflowers of CuO, together with a certain amount of $Cu_2O$, were generated. When the current density was increased to over 1 mA $cm^{-2}$, $Cu(OH)_2$ rather than CuO nanoneedles was obtained. The increase in current density facilitated the formation of $Cu(OH)_2$ and prevented the generation of the side product $Cu_2O$. The optimized anodization conditions for fabricating $Cu(OH)_2$ nanoneedles or nanotubes are listed in Table 2. In addition, $Cu(OH)_2$ nanoneedles can be readily converted to CuO nanoneedles by annealing at 200 °C for 3 h under a nitrogen atmosphere[88].

The formation of nanoneedles by the anodization of Cu in KOH or NaOH electrolytes was further confirmed in subsequent studies[89-103]. Allam and Grimes found that the reaction of Cu foil in an aqueous KOH electrolyte was pH dependent[89]. No film was formed on the Cu surface when the reaction was performed in KOH solutions with pH ≤ 10. Zhang and Wang explored the anodization of electrodeposited Cu films in a 3 mol $L^{-1}$ solution NaOH at different current densities[90]. They found that the anodic films prepared at a lower current density were $Cu_2O$ with polyhedral structures, while those prepared at a higher current density were $Cu(OH)_2$ with a randomly packed nanowire (or nanoneedle) structure. This was in reasonable agreement with the experimental findings of the Shi group[88]. Moreover, different annealing environments and temperatures were found to result in the formation of different CuO and/or $Cu_2O$ nanostructures when the $Cu(OH)_2$ nanoneedles were annealed[92,104]. For instance, when anodized Cu foam was heated under a nitrogen atmosphere at 150 °C for 3 h and at 200 °C for 3 h, CuO nanowires were formed on the Cu foam. In contrast, when the anodized sample was heated in air at 200 °C for 15 min, CuO nanosheets were generated on the Cu foam[91]. When the Cu foam was anodized at 30 mA $cm^{-2}$ in a 3 mol $L^{-1}$ aqueous KOH solution at 40 °C, leaf-like $CuO/Cu_2O$ nanosheets were obtained directly[105]. Recently, Anantharaj and coworkers found that a much denser $Cu(OH)_2$/CuO nanoneedle array could be obtained within just 80 s by the anodization of Cu foil using a conventional three-electrode system-based potentiostatic (at 0.864 V *vs.* a RHE) method in 1.0 M KOH[106,107]. Increasing the pH of KOH electrolytes led to an increase in the average length of the $Cu(OH)_2$/CuO nanoneedles.

### Nanoporous and leaf-like nanoarchitectures

Inspired by the fact that the anodization of metals like Ti in fluoride-containing media can lead to the formation of nanoporous/nanotubular structures, the Grimes group studied the anodization of Cu foil in halide-containing solutions in 2011 in an attempt to obtain nanoporous copper oxide films[89]. They investigated the combined effect of KOH and $NH_4Cl$ on Cu anodization and found that no porous structure could be obtained using $NH_4Cl$-based electrolytes. This result was also verified in a more recent study[108]. The Grimes group[89] discovered that a nanoporous structure appeared on the entire Cu surface after the Cu foil was anodized at 6 V for 300 s in an aqueous electrolyte containing 0.15 mol $L^{-1}$ KOH and 0.1 mol $L^{-1}$ $NH_4F$. When the KOH concentration was increased to 0.2 mol $L^{-1}$ while maintaining all other conditions, anodic products with porous microspheroids were obtained. However, when Cu thin films of ~450 nm

**Table 2. Products formed by anodization of Cu at 1.5 mA $cm^{-2}$ in media with different concentrations of KOH ($C_{KOH}$) and at different temperatures (*T*)[88]. Reproduced from Ref.[88] with permission from the American Chemical Society**

| *T* (°C) | $C_{KOH}$, 2.0 mol $L^{-1}$ | $C_{KOH}$, 2.5 mol $L^{-1}$ | $C_{KOH}$, 3.0 mol $L^{-1}$ | $C_{KOH}$, 3.5 mol $L^{-1}$ |
|---|---|---|---|---|
| 2 ± 2 | $Cu(OH)_2$ nanoneedles | $Cu(OH)_2$ nanoneedles | $Cu(OH)_2$ nanoneedles | $Cu(OH)_2$ nanoneedles |
| 15 ± 2 | $Cu(OH)_2$ nanoneedles | $Cu(OH)_2$ nanoneedles | $Cu(OH)_2$ nanotubes | $Cu(OH)_2$ nanotubes |
| 28 ± 2 | $Cu(OH)_2$ nanoneedles | $Cu(OH)_2$ nanotubes | $Cu(OH)_2$ nanotubes | CuO nanoparticles |

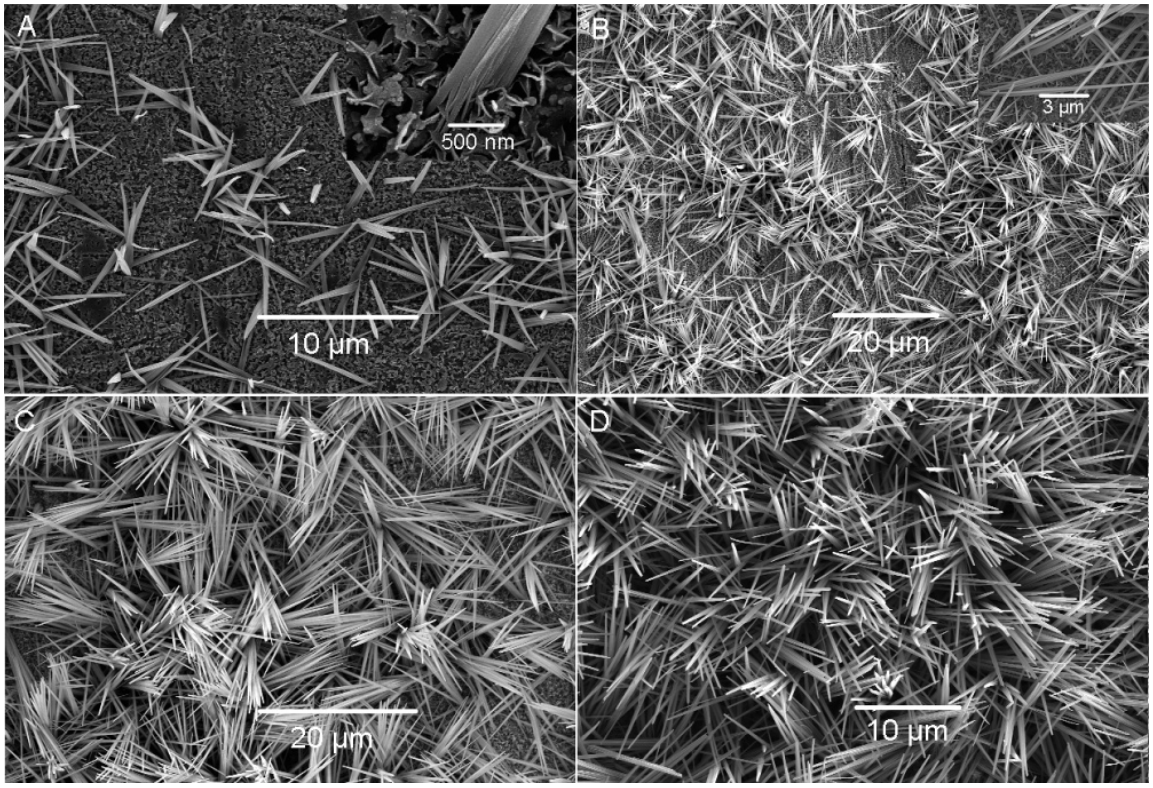


**Figure 3.** SEM images of as-prepared $Cu(OH)_2$ nanoneedles formed at 1.5 mA $cm^{-2}$ in a 2.0 mol $L^{-1}$ KOH solution at *T* = 28 ± 2 °C for different anodization times: (A) 300 s; (B) 500 s; (C) 1000 s; (D) 1500 s[88]. Reproduced from Ref.[88] with permission from the American Chemical Society.

thickness were anodized in the same aqueous electrolytes containing 0.1 mol $L^{-1}$ $NH_4F$ under similar anodization conditions, the anodic products still showed nanowire structures[109].

The Grimes group also showed that changing the electrolyte solvent from water to EG still did not produce the nanoporous/nanotubular structures like those found after Ti anodization[89]. Nevertheless, the formation of leaf-like nanoarchitectures with a thickness of ~160 nm was observed upon the anodization at 30 V for 300 s of Cu foil in an EG electrolyte containing 0.15 mol $L^{-1}$ KOH, 0.1 mol $L^{-1}$ $NH_4F$ and 3% $H_2O$. Increasing the KOH concentration to 0.2 mol $L^{-1}$ led to the growth of thicker oxide films of ~500 nm with the same leaf-like morphology[89]. However, Jerez *et al.* obtained nanoporous mixed $Cu_2O$/CuO films when the Cu anodization was conducted at a relatively lower temperature (5 °C) in similar EG electrolytes[110]. Furthermore, the current-time transients during potentiostatic anodization were similar to those observed for Ti anodization. Wang *et al.* found that the calcination temperature played a key role in determining the final morphology of the anodization products[111]. Nanoporous $Cu_2O$ films were formed by anodization in

an EG electrolyte containing 0.75 wt.% KOH, 0.20 wt.% NaF and 3.0 wt.% $H_2O$. The formation of a dense array of CuO nanowires embedded within the surface of the $Cu_2O$ layer was observed after the anodized films were annealed at 400 °C for 60 min.

Shu *et al.* also prepared leaf-like copper oxide nanosheets in the NaOH-NaCl-polyethylene glycol (PEG) aqueous electrolyte system[112,113]. They found that higher anodization temperatures were required for generating copper oxide nanosheets in NaOH-NaCl-PEG electrolytes. No oxide film was observed on the Cu surface when the anodization temperatures were lower than 50 °C[112]. Furthermore, they found that the addition of ammonium molybdate (AM) in the NaOH-NaCl-PEG solutions inhibited the $Cu \rightarrow Cu^+$ oxidation reaction, resulting in the formation of single-phase CuO nanosheet films. Typically, in an aqueous solution containing 1 mol $L^{-1}$ NaOH, 2.5 mol $L^{-1}$ NaCl, 1 g $L^{-1}$ PEG and 20 g $L^{-1}$ AM, single-phase CuO nanosheets were obtained directly on Cu foam when it was anodized at a constant current of 10 mA $cm^{-2}$ at 65 °C. These grown nanosheets were ~2 μm in size with a thickness of ~30-50 nm[113].

### Other nanostructures and anodization products

Since the aqueous solutions of carbonate salts of alkali metals are weakly alkaline, they have also been used as electrolytes for Cu anodization in addition to the commonly used NaOH or KOH solutions. Stępniowski *et al.* investigated the growth of nanostructured anodic films on Cu in 0.1 mol $L^{-1}$ $K_2CO_3$[114-116], 0.1 mol $L^{-1}$ $Na_2CO_3$[117] and 0.01 mol $L^{-1}$ $KHCO_3$[118] solutions, respectively. The resultant anodic films formed in these carbonate-based electrolytes typically had a nanorod-like morphology. Moreover, in a 0.5 mol $L^{-1}$ potassium oxalate solution, the Cu anodization led to the formation of copper oxalate and a CuO complex film with rough and porous microstructures[119]. When the Cu anodization was completed in a room-temperature ionic liquid, 1-butyl-3-methylimidazolium hexafluorophosphate, containing *N*-butyl-*N*-methylpyrrolidinium iodide[120], or in a potassium iodide electrolyte[121], crystalline cuprous iodide (CuI) thin films were obtained. Interestingly, after anodization in a 0.1 mol $L^{-1}$ $Na_2WO_4$ solution at 3 V for 5 min, anodic films with cauliflower-like structures appeared on the Cu surface, which were confirmed to be $CuWO_4$ and CuO composites[122]. Similarly, Cu anodization at 10 V in a mixed aqueous solution containing 0.05 mol $L^{-1}$ $NaH_2PO_4$ and 0.05 mol $L^{-1}$ $Na_2HPO_4$ resulted in the growth of leaf-like copper phosphate films[123]. The copper phosphate films showed high catalytic activity for the Fenton oxidative degradation of dyes. Moreover, copper(II) myristate films with a "star-like" structure were found to be formed by Cu anodization at a relatively high voltage (100 V) in a nonaqueous electrolyte (0.1 mol $L^{-1}$ myristic acid and 0.1 mol $L^{-1}$ tetraethylammonium tetrafluoroborate in methanol)[124]. In particular, Lu *et al.* added 0.07 mol $L^{-1}$ cetyltrimethylammonium bromide (CTAB) into a 3 mol $L^{-1}$ KOH aqueous solution and explored Cu anodization in this electrolyte[125]. Because CTAB served as a template for the formation of the nanofilms, graphene-like $Cu(OH)_2$ nanofilms were obtained by anodization. Consequently, graphene-like CuO nanofilms were successfully prepared after the common thermal treatment of $Cu(OH)_2$ films. Recently, Liu *et al.* fabricated tremella-like $Cu_xO@Cu_xS$ nanosheets on copper mesh by anodization in a 0.5 mol $L^{-1}$ $Na_2S$ solution with a constant current of 5 mA at 0 °C and a subsequent annealing process at 200 °C in air[126]. The synthesized organic-free tremella-like $Cu_xO@Cu_xS$ nanosheets exhibited superhydrophilicity and underwater superoleophobicity.

## Applications

Copper oxides (CuO and $Cu_2O$) have attracted significant attention for a wide variety of applications due to their relatively low cost, nontoxicity, abundance and high chemical stability. As indicated above, numerous research efforts have focused on tuning the nanostructure and function of copper oxide-based materials by anodization, which has led to the discovery of many fascinating properties and applications. In addition to the PEC and supercapacitor applications commonly encountered, copper oxide-based materials have found applications in sensors[43,109,119,127,128], pH-controllable water permeation[93], superhydrophobic anticorrosion

coatings[94,95,129], oil/water separation[122] and surface-enhanced Raman scattering substrates[108].

*PEC applications*

In contrast to iron oxides, copper oxides (CuO and $Cu_2O$) are p-type semiconductors and are thus suitable for use as photocathode materials. Compared to CuO, $Cu_2O$ is a more attractive photocatalyst for PEC hydrogen production with a direct bandgap of 2 eV and a corresponding theoretical photocurrent of -14.7 mA $cm^{-2}$ and a light-to-hydrogen conversion efficiency of 18.7% based on the AM1.5 spectrum[130]. The key issue facing $Cu_2O$ as a photocathode for water reduction is its instability in aqueous solutions under illumination since its redox potentials for reduction ($Cu_2O$ to Cu) and oxidation ($Cu_2O$ to CuO) are located within the bandgap of $Cu_2O$. Zhang and Wang prepared $Cu_2O$-CuO composite films with nanoneedle morphologies by anodization of the electrodeposited Cu film and subsequent annealing[90]. The best photocathode material among all materials fabricated using different conditions was a $Cu_2O$-CuO composite with $Cu_2O$ in the (220) orientation, which exhibited a high photocurrent of -1.54 mA $cm^{-2}$ at 0 V *vs.* a RHE with a greatly enhanced stability at a mild pH under illumination of AM 1.5 G. The good PEC activity of these composite materials could be attributed to the top layer of CuO in the composites, which not only minimized the $Cu_2O$ photocorrosion but also acted as a recombination inhibitor for the photogenerated electrons and holes from $Cu_2O$[90].

Similarly, a $Cu_2O$-CuO composite film on a Cu substrate, in the form of CuO nanowires embedded in a dense layer of $Cu_2O$, was obtained by Wang *et al.*[111]. This composite film was able to generate 0.360 mA $cm^{-2}$ of photocathodic current density upon visible-light illumination and could retain its photocathodic current density after being used and kept for a month. Furthermore, the $Cu_2O$-CuO composite film could be fabricated only by anodization in NaOH-NaCl-PEG electrolytes[112]. The obtained nanosheet arrays composed of $Cu_2O$ and CuO yielded optimal PEC performance with a photocurrent of ~0.4 mA $cm^{-2}$. Joya *et al.* prepared a leaf-type copper oxide film on a Cu substrate by constant-current anodization of Cu in a carbonate buffer solution (0.2 M, pH ~11)[131]. The as-anodized copper oxide film was found to be a stable and high-performance water oxidation electrocatalyst. Oxygen evolution started at a very low overpotential (320 mV) and an oxygen evolution current density of 10 mA $cm^{-2}$ was achieved at 1.68 V (*vs.* a RHE). Its high catalytic activity was related to its leaf-type convex nanostructured surface morphology and the presence of carbon in the film. In addition, the $Cu_2O$ film prepared by an anodization-based method also presented excellent photocatalytic activities for water oxidation and oxygen evolution under visible light[132].

*Supercapacitors*

Over the past decade, copper oxides have experienced a surge in interest for their application in supercapacitors owing to the rich variety of their electrochemical responses and nanostructures[133]. Because copper oxides/hydroxides are grown in situ on Cu substrates by the anodization route, unlike powder-type active materials, they can be directly employed as electrodes in supercapacitors without using any binder. Moreover, nanostructured copper oxides/hydroxides with various morphologies can also be obtained by anodization, as described above. Consequently, copper oxides/hydroxides prepared by anodization have been studied extensively for use in supercapacitors[91,96,98-101,103,105,113,125,134].

Generally, nanostructured CuO, $Cu_2O$ or $Cu(OH)_2$ films (e.g., nanowires and nanosheets) obtained by the anodization technique have produced cyclic voltammograms with ill-defined or broad redox peaks in alkaline solutions, although their capacitances were believed to originate from Faradaic redox reactions[91,98,103,105]. Figure 4 displays the typical cyclic voltammograms of CuO nanowires, nanosheets and nanoflowers in a 6.0 mol $L^{-1}$ KOH solution. It has been proposed that the following redox reactions of these

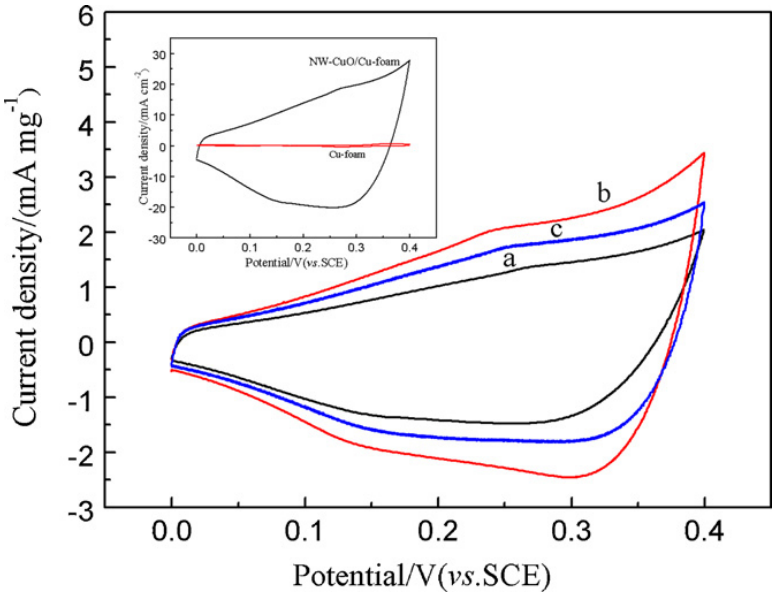


**Figure 4.** Cyclic voltammograms of (a) CuO nanowires, (b) CuO nanosheets and (c) CuO nanoflowers recorded in a 6.0 mol $L^{-1}$ KOH solution at a scan rate of 20 mV $s^{-1}$. The inset shows the cyclic voltammograms of the Cu foam substrate and the CuO nanowires on the Cu foam electrode with the same geometrical area of 1 $cm^2$ [91]. Reproduced from Ref.[91] with permission from Elsevier.

copper oxides/hydroxides in alkaline solution may be involved in the transition between Cu(I) and Cu(II) species:

$$½Cu_2O + OH^- \leftrightarrow CuO + ½H_2O + e^- \quad (3)$$

$$½Cu_2O + ½H_2O + OH^- \leftrightarrow Cu(OH)_2 + e^- \quad (4)$$

$$CuOH + OH^- \leftrightarrow CuO + H_2O + e^- \quad (5)$$

$$CuOH + OH^- \leftrightarrow Cu(OH)_2 + e^- \quad (6)$$

The broad redox peaks in their cyclic voltammograms, as illustrated in Figure 4, could be attributed to the overlap of the redox processes expressed in Equations 3-6[91]. These nanostructured copper oxides/hydroxides in alkaline solutions can exhibit relatively high specific capacitances and good cycling stability. For example, leaf-like CuO-$Cu_2O$ nanosheets on Cu foam showed a high capacitance of 1.954 F $cm^{-2}$ and excellent cycling stability without a decrease in capacitance after 5000 cycles[105]. The anodized $Cu(OH)_2$ nanorods delivered a high capacitance of 260 F·$g^{-1}$ (at 5 mV $s^{-1}$) and retained 92.0% of the initial capacitance after 5000 charge-discharge cycles[134]. However, these copper oxides/hydroxides had relatively narrower operating potential windows (e.g., from 0 to 0.4 V, Figure 4). This may be due to their low oxygen evolution potential in alkaline solutions. Furthermore, their coulombic efficiency was comparatively low[105].

As mentioned above, Lu *et al.* successfully fabricated graphene-like CuO nanofilms on Cu foam by *in-situ* anodization[125]. As shown in Figure 5A-C, the fabricated electrode was comprised of interconnected CuO nanofilms with open mesopores. Furthermore, the individual CuO nanofilms with a thickness of ~2 nm had a graphene-like flexible and folded structure [Figure 5D]. Unlike the aforementioned copper

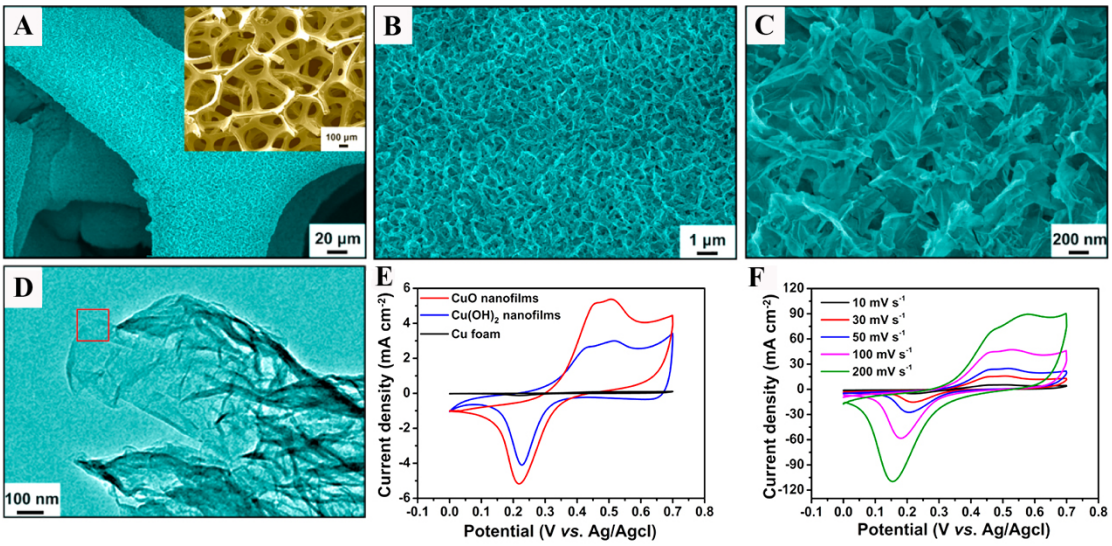


**Figure 5.** Morphologies of CuO nanofilms: (A-C) SEM images taken at different magnifications; (D) TEM image. Cyclic voltammograms of (E) different electrodes at 10 mV $s^{-1}$ and (F) CuO nanofilm electrode at various scan rates. The inset of (A) shows an SEM image of the bare Cu foam[125]. Reproduced from Ref.[125] with permission from the American Chemical Society.

oxides/hydroxides, the CuO nanofilms displayed well-defined redox peaks [Figure 5E and F], corresponding to the transition between Cu(I) and Cu(II) species (Equation 3). The dramatically different electrochemical response was primarily attributed to the ultrathin graphene-like structure with short pathways for ion transport. Moreover, the CuO nanofilms exhibited a much higher specific capacitance (919 $F{\cdot}g^{-1}$ at 1 $A{\cdot}g^{-1}$) and good cycling stability (7% capacitance loss after 5000 cycles). In addition, they showed excellent photocatalytic activities. More recently, Gong *et al.* prepared needle-like $Cu(OH)_2$ nanowires on nanoporous Cu by anodization, with the cyclic voltammograms also exhibiting a pair of very obvious redox peaks[103]. Their nanoporous Cu with uniform and continuous porous structures was fabricated by dealloying a Cu-Zr-Ni-Be quaternary amorphous alloy in mixed acid solutions. The reason why the needle-like $Cu(OH)_2$ nanowires showed distinct redox peaks may be related to the nanoporous Cu substrate.

## ZINC

Because alkaline batteries with Zn electrodes are manufactured commercially and used on a large scale, the anodization behavior of Zn in alkaline solutions has been widely investigated as early as the 1950s[135-137]. Early work primarily focused on the understanding of the anodic ZnO formation processes and the related electrochemical reactions in alkaline solutions. In contrast, relatively little information on the microscopic morphologies of the anodic films has been published[138-143]. Over the past two decades, there has been increasing interest in the anodic fabrication of nanostructured ZnO with various morphologies owing to its many promising applications. For Zn anodization, it is noteworthy that even small changes in electrolyte composition or anodization voltage may lead to dramatic changes in both the morphology and structure of the as-anodized films.

### Nanoneedles, nanorods, nanowires and nanotubes

Similar to the case of $Cu(OH)_2$ nanoneedles discussed above, the first report on the anodization preparation of ZnO nanoneedles was also published by the Shi group in 2006[144]. They demonstrated that highly oriented ZnO nanoneedle arrays could be prepared by the anodization of Zn foil in a saturated zincate [$Zn(OH)_4^{2-}$] solution at room temperature. The electrolyte used was a freshly prepared saturated aqueous

zincate solution, which was prepared by adding 10 mL of 1.0 mol $L^{-1}$ $Zn(NO_3)_2$ into 10 mL of 4.0 mol $L^{-1}$ KOH with vigorous stirring and then removing the precipitate by centrifugation. Crystalline ZnO nanoneedle arrays were obtained by anodization in a freshly prepared 0.5 mol $L^{-1}$ zincate aqueous solution at 0.3 mA $cm^{-2}$ and 1.5 C $cm^{-2}$. As shown in Figure 6, these ZnO nanoneedles were aligned perpendicular to the Zn substrate surface and coated on the substrate uniformly and compactly, typically having a length of 550-650 nm with a tip diameter of 10-15 nm and a root diameter of 50-60 nm. They found that the concentration of zincate may play a key role in the formation of anodic ZnO nanoneedles. The nanoneedles were not formed in electrolytes with low zincate concentrations. The anodization of Zn in a pure aqueous KOH solution (2.0 M) only led to the dissolution of Zn in the solution[144]. Subsequent studies also demonstrated that ZnO nanoneedles could be formed by anodization in a concentrated NaOH solution (4.0 M), whereas nanoporous ZnO films were obtained in 0.1 mol $L^{-1}$ NaOH (KOH) solution, since the zincate was formed in concentrated alkaline solutions[145-147].

Several years later, Hu and coworkers reported the rapid synthesis of ultralong ZnO nanowire films by anodization in a slightly basic solution[148]. They found that high-aspect-ratio nanowire arrays of tens of microns in length and 30-100 nm in diameter can be formed on Zn foil rapidly by anodizing in an aqueous 5-50 mM $KHCO_3$ solution at room temperature. The as-anodized nanowires were demonstrated to be highly crystalline materials that may have the composition $Zn(OH)_n(CO_3)_m$ and could be readily converted to ZnO nanowires by annealing at 250 °C for 1 h in air. Figure 7 shows the morphological evolution during anodization of Zn at 10 V. In the initial stages of anodization, the Zn foil was dissolved to form irregular, discrete pits over the surface of the metal [Figure 7a]. Furthermore, nanoflower-like products appeared inside the pits [Figure 7A]. As the anodization time increased, the morphology of the anodic films was transformed gradually from discrete nanoflower-like structures to a uniform film of aligned nanowires [Figure 7]. Numerous follow-up studies further revealed that the nanowire length and diameter and density of the nanoflower-like structures were directly proportional to the anodization time[149-154]. In addition, nanowires can be grown at a rather high rate (~1.3 μm $min^{-1}$)[149-154] in an aqueous $KHCO_3$ solution.

In addition to the aqueous $KHCO_3$ solution, other bicarbonate electrolytes, including $NaHCO_3$ and $NH_4HCO_3$, have also been utilized in the anodization fabrication of ZnO nanowires[155-160]. Miles *et al.* thoroughly investigated the anodization behavior of Zn in aqueous $KHCO_3$, $NaHCO_3$ and $NH_4HCO_3$ solutions[155]. They demonstrated that the growth of high-aspect-ratio nanowires by Zn anodization was possible using the three bicarbonate electrolytes. The authors found that, for the very thick nanowire films (> 50 μm), hierarchical three-dimensional nanowire structures instead of aligned nanowires were typically formed. Furthermore, the nanowire growth rates in $NaHCO_3$ and $NH_4HCO_3$ electrolytes were noticeably higher than those in the $KHCO_3$ solution. Under the optimized conditions, growth rates as high as 3.2 μm $min^{-1}$ could be attained, even well above those of AAO under high-field anodization conditions[161-163]. It is noteworthy that short nanowire structures were also obtained in an aqueous $NH_4F$ solution[164] and in an electrolyte based on EG and $NH_4F$[165].

In work by Katwal *et al.*, it was observed that nanotubes appeared at the edges (< 5% of the area) of the Zn foil, although the foil was covered predominantly by nanowires [Figure 8A], while the Zn anodization was performed first at 10 V in a 6.8 mM $NaHCO_3$ solution, followed by a second anodization at 20 V in a 0.2 mM $NaHCO_3$ solution[166]. Nevertheless, when the anodization was conducted only once in a mixed solution of 6.8 mM $NaHCO_3$ and 5.7 mM $Na_2CO_3$ at 10 V, the nanotube coverage improved remarkably to ~50%, as shown in Figure 8B and C. The obtained nanotube-nanowire hybrid architectures with a length of ~14 μm were formed after 10 min of anodization. The diameters of the nanotubes ranged typically from ~100 to ~300 nm and the pore diameters were from ~10 to ~200 nm [Figure 8D][166]. Similar results were

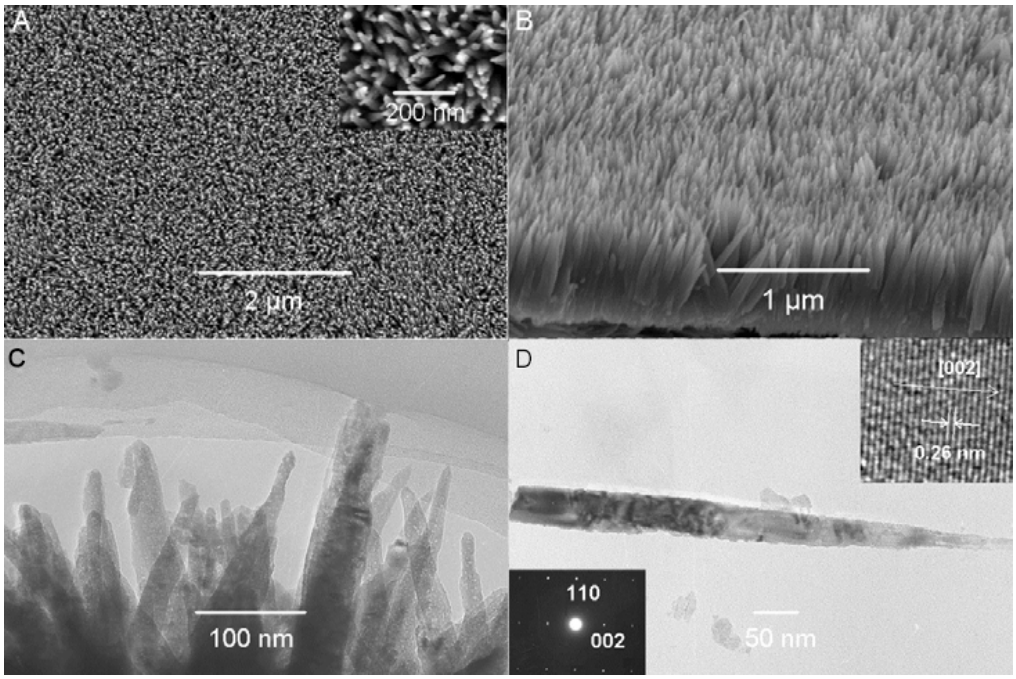


**Figure 6.** (A and B) SEM and (C and D) TEM images of as-prepared ZnO nanoneedles. The inset of (A) shows a magnified view. The inset of (D) shows the SAED and HR-TEM pattern of a ZnO nanoneedle[144].Reproduced from Ref.[144] with permission from IOP Publishing.

obtained later in a mixed solution of $NaHCO_3$ and $Na_2CO_3$ by other authors[167]. More recently, Batista-Grau and coworkers explored the influence of hydrodynamic conditions (from 0 to 5000 rpm) and the addition of ethanol or glycerol to the $NaHCO_3$ solution on the morphology of the products formed during the Zn anodization process[168,169]. They showed that the hydrodynamic conditions during anodization facilitated the formation of ordered ZnO nanowires along the surface. A significant influence on the morphology, as a result of the addition of ethanol or glycerol, was observed. In glycerol-containing $NaHCO_3$ electrolytes, ZnO nanotubes, nanospheres and nanosponges were also formed in addition to nanowires[169]. Furthermore, hierarchically structured self-organized ZnO/ZnS nanotubes can be synthesized by the anodization of Zn in a $Na_2S$- or $(NH_4)_2S$-based electrolyte containing a small amount of $NH_4F$[170-172].

### Nanoporous films

Several reports have mentioned that, in oxalic acid electrolytes, nanoporous ZnO thin films were typically formed by the electrochemical anodization of Zn[173,174]. Interestingly, ZnO porous structures on Zn metal were also obtained by Zn anodization just using deionized/distilled water as an electrolyte at room temperature[175,176]. As the deionized water itself was slightly acidic (pH 5.8), the Zn anodization could be carried out in water without the need for the addition of any extra electrolyte[175]. The morphologies of the ZnO thin films were found to be highly dependent on the anodization voltages[176].

As described above, Zn anodization in a concentrated NaOH solution led to the formation of ZnO nanoneedles[145]. In contrast, it was also reported that nanoporous anodic ZnO films could be produced in dilute NaOH solutions (< 1 M)[147,177-179]. For example, a porous anodic film with a thickness of ~10 μm was obtained by anodization in a 0.1 mol $L^{-1}$ NaOH solution at 20 V for 90 min, which consisted of crystalline ZnO with a straight cellular structure similar to that of AAO[177]. It was suggested that the addition of EG to the NaOH solution could improve the film properties and current efficiency of anodization[177]. When a

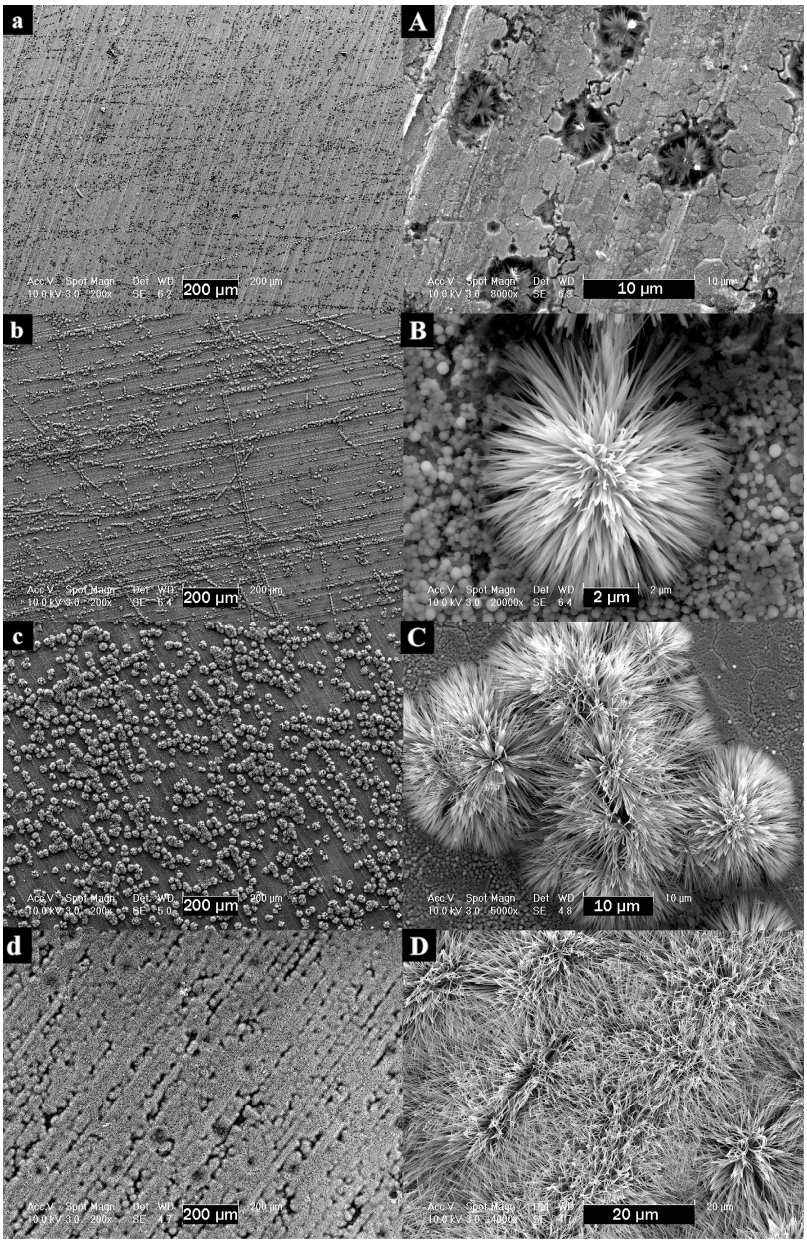


**Figure 7.** Morphological evolution of anodized Zn foils at 10 V for selected periods. (a-d) refer to 1, 5, 10 and 20 min anodization times, respectively. (A-D) show the corresponding magnified images[148]. Reproduced from Ref.[148] with permission from the American Chemical Society.

1 mol $L^{-1}$ NaOH aqueous electrolyte was employed, relatively low anodization voltages (2 or 4 V) were adopted to fabricate nanoporous ZnO films. Furthermore, the prepared porous films had relatively disordered nanoporous structures in comparison with the films produced in a 0.1 mol $L^{-1}$ NaOH solution[179]. Additionally, the Schmuki group found that Zn anodization in a fluoride electrolyte containing 2-methyl-1,3-propanediol at low temperatures (-2 to -30 °C) resulted in hierarchically structured self-organized porous films[180]. The as-grown film was confirmed to be $ZnF_2$-rich amorphous ZnO.

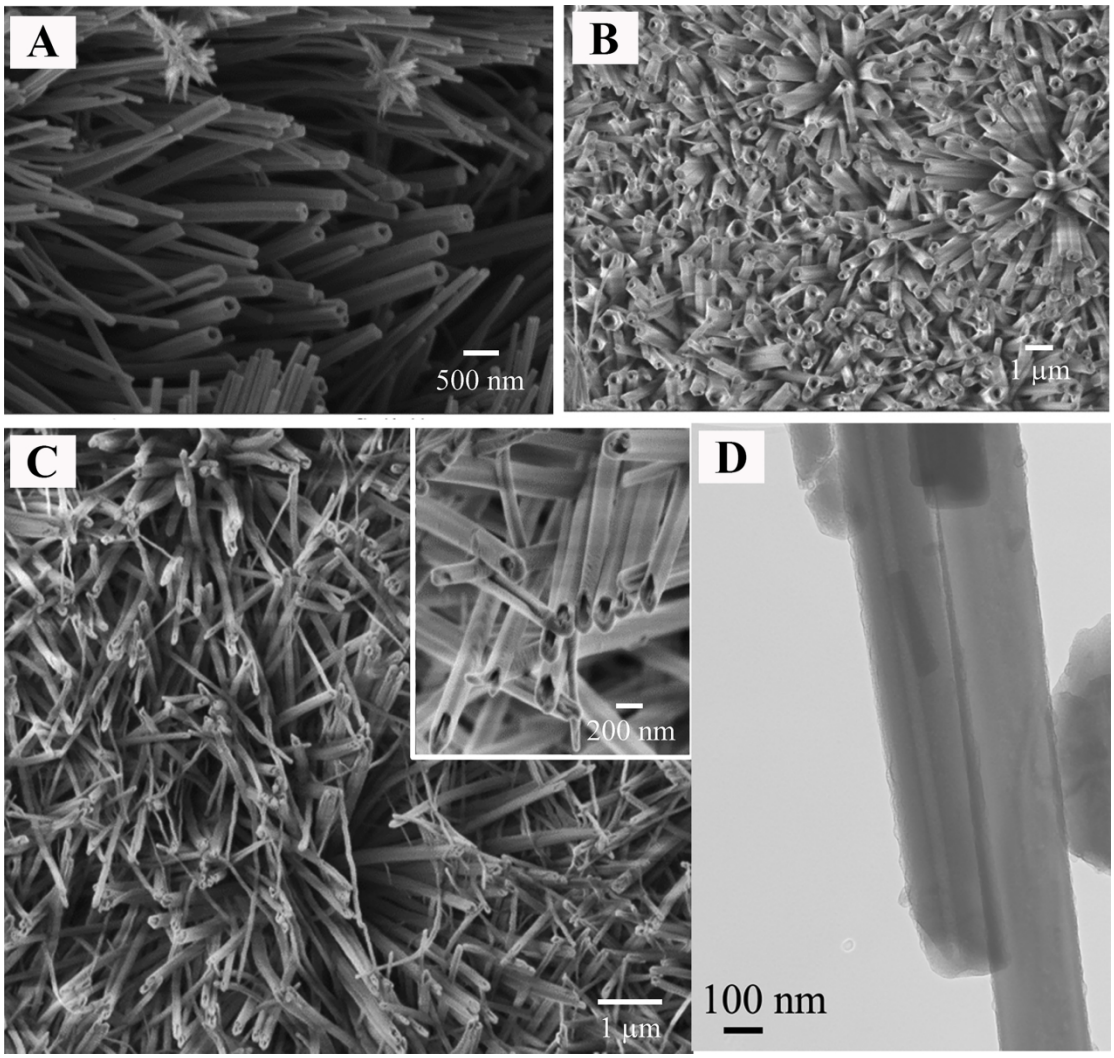


**Figure 8.** SEM images of a zinc oxide nanotube-nanowire mixed structure fabricated in an aqueous electrolyte containing (A) only $NaHCO_3$, in which < 5% of the substrate area was covered with nanotubes, and (B and C) both $Na_2CO_3$ and $NaHCO_3$. (D) TEM image showing a nanotube and a nanowire[166]. Reproduced from Ref.[166] with permission from the American Chemical Society.

### Other nanostructures and anodization products

So far, it has been shown that the compositions of the electrolytes used in anodization play a particularly influential role in determining the nanostructures of anodic ZnO films. Apart from the commonly used NaOH/KOH and bicarbonate electrolytes, other electrolytes, such as silicate-based solutions[181], $H_2SO_4$ solutions[182], methanol solutions containing HF and water[183], mixed solutions of $(NH_4)_2SO_4$ and $NH_4Cl$[184], $H_3PO_4/NH_4H_2PO_4$ solutions[185] and mixed solutions of $(NH_4)_2SO_4$ and NaOH[186], could also be employed to make nanostructured anodic films by Zn anodization. In 2008, Kim and Choi utilized $H_2SO_4$ solutions in ethanol instead of in water to fabricate ZnO films by anodization[182]. Unlike the formation of hexagonal etched arrays or the stair-like morphology of ZnO obtained in aqueous $H_2SO_4$ solutions, anodization in a $H_2SO_4$ solution in ethanol led to the formation of self-assembled ZnO stripes consisting of 800 nm polygonal flakes, which may be attributed to the water-selective dissolution of ZnO and the hydrodynamic flow of water by convection[182]. In 0.1 wt.% HF solutions in a mixture of methanol and water, ZnO nanoflowers composed of hundreds of sheet-like nanopetals were found to be grown on a Zn substrate after a potentiostatic anodization of 15 min[183]. In contrast, in a mixed solution of 0.2 mol $L^{-1}$ $(NH_4)_2SO_4$ and

0.2 mol $L^{-1}$ $NH_4Cl$, large-scale ZnO sunflower structures with a diameter of 400-500 μm were formed[184]. In addition, the formation of leaf-like ZnO nanoflakes by Zn anodization in a mixture of $(NH_4)_2SO_4$ and NaOH was reported[186]. Most interestingly, zinc phosphate microporous spheres with diameters of 5-23 μm were obtained by the potentiostatic anodization of Zn in a 0.2 mol $L^{-1}$ $H_3PO_4$ or $NH_4H_2PO_4$ solution at 1 V[185]. More recently, Heo and coworkers reported a facile anodization method for synthesizing zinc ricinoleate (a deodorizing agent)[187]. Zinc ricinoleate powders with a spherical morphology were prepared by the anodization of Zn foil in an electrolyte containing ricinoleic acid, water and ethanol (4:4:2 v/v).

## Applications

Zinc oxide (ZnO) is a well-known piezoelectric material and also an n-type semiconductor with a wide direct bandgap (~3.37 eV). It offers many unique and promising properties, such as a large exciton binding energy (60 meV), high electron mobility, good photocatalytic activity, excellent thermal and chemical stability, large piezoelectric constant and easily modified electric conductivity[188]. Therefore, nanostructured ZnO materials have been studied for many potential applications, including photoluminescence[142,146,189], gas sensors[173,190,191], biological applications[166,167,192], photodetectors[151], control of surface wettability[152,183,193], photocatalysts[141,177,186,194-198], dye-sensitized solar cells[149] and PEC water splitting[168-171,199,200].

Unsurprisingly, the majority of research efforts have focused on the PEC applications of ZnO due to its efficient PEC response. For example, the Schmuki group fabricated hierarchically structured self-organized ZnO nanotubes by Zn anodization in a sulfide-based aqueous electrolyte containing a small amount of $NH_4F$ and studied their PEC water splitting performance[170]. The highest photocurrent values (~1.7 mA $cm^{-2}$) were found for the fabricated ZnO nanotubes (containing a certain amount of ZnS) with a length of 3 μm annealed at 375 °C under an external bias of -0.14 V *vs.* Ag/AgCl in a sacrificial polysulfide electrolyte. They suggested that the excellent PEC properties could be ascribed to the sacrificial polysulfide electrolyte, which hindered the corrosion/photocorrosion of the ZnO/ZnS structure[170]. Huang *et al.* demonstrated that anodized ZnO with different nanostructures exhibited markedly different PEC properties[199]. The photoanode made of ZnO nanowires had a photocurrent density of 0.32 mA $cm^{-2}$ at 0.5 V *vs.* a SCE under 100 mW $cm^{-2}$ illumination, ~1.9 times higher than that of anodes made of nanosheets (0.17 mA $cm^{-2}$ under the same conditions). The superior PEC performance of nanowires probably resulted from single crystals with a preferred orientation of (002), higher carrier concentration and lower charge transfer resistance relative to polycrystalline nanosheets. Furthermore, the stability of the anodized ZnO samples was higher than that of other samples prepared by sol-gel or chemical bath processes[199]. Sanz-Marco *et al.* synthesized ZnO/ZnS nanotubular structures by anodization in a glycerol-based electrolyte containing $Na_2S$ and $NH_4F$ under hydrodynamic conditions[171]. The PEC properties of the resultant films were found to be heavily dependent on the anodization voltage and the electrode rotation speed during anodization. Optimal PEC performance was observed for samples anodized at 40 V and at 1000 rpm, which exhibited a 71% increase in photocurrent density for PEC water splitting in comparison to those anodized at 20 V and 1000 rpm[171].

Very recently, as mentioned earlier, Batista-Grau *et al.* fabricated different nanostructured ZnO electrodes by anodization in $NaHCO_3$ and $NaHCO_3$ solutions containing ethanol or glycerol under hydrodynamic conditions[168,169]. Their experimental results established that the obtained ZnO nanostructures presented high photocurrent density response during water splitting measurements in a sacrificial polysulfide electrolyte. In particular, the samples anodized at 5000 rpm in $NaHCO_3$ solutions showed a ~159% improvement in the photocurrent density response compared to those anodized under stagnant conditions[168]. It was observed that when 10% v/v of ethanol or 25% v/v of glycerol was added to the aqueous $NaHCO_3$ electrolyte, the photocurrent density response for the electrodes obtained in the organic solvent containing an electrolyte under stagnant conditions was greatly increased. The photocurrent density

response of the ZnO electrode anodized in a $NaHCO_3$ electrolyte containing 10% v/v ethanol (0.34 mA $cm^{-2}$) was twice that of the sample anodized under the same conditions in an aqueous $NaHCO_3$ electrolyte (0.17 mA $cm^{-2}$)[168,169]. Finally, it should be mentioned that, unlike iron and copper oxides, ZnO materials have rarely been investigated as electrode material for supercapacitors, likely due to the absence of variable oxidation states for Zn. There is only one publication reporting the specific capacitance of anodized ZnO nanorods but without providing any other performance parameters[154].

## CONCLUSION AND OUTLOOK

This review provides a comprehensive survey of the current research progress in the field of anodization of transition metals, with specific emphasis on the growth process of nanostructured anodic films on Fe, Cu and Zn metals and their corresponding applications. Typically, as-anodized films on Fe are essentially amorphous, whereas the anodic films prepared by Cu and Zn anodization are relatively crystalline. Anodic films with various nanostructures, such as nanopores, nanotubes, nanoflowers, nanoneedles and nanowires, have been successfully produced in different electrolytes. We conclude that the anodization conditions, including anodization voltage, anodization duration, electrolyte composition, the organic solvent, anodization bath temperature and water content, have profound effects on the morphologies of anodic films. Fluoride-containing solutions were found to be a universal type of electrolyte for the formation of nanostructured anodic films on transition metal surfaces. Moreover, in some electrolytes containing special anionic species, including iodide, phosphate and sulfide, the as-anodized products were metal iodides (or phosphates or sulfides) instead of metal oxides/hydroxides. The anodized films on transition metals have found widespread applications in PEC water splitting, photocatalysis, lithium-ion batteries, supercapacitors and biomaterials[201,202].

At present, anodization has become a widely used technique for preparing metal oxides with various nanostructures. In addition to transition metals, some non-transition metals, like tin, have also been anodized to fabricate nanomaterials with various unique properties[203-208]. However, compared with the highly ordered AAO, the anodized films on transition metals, such as Fe, Cu and Zn, showed fewer perfect nanostructures with relatively low degrees of ordering. More recently, Yanagishita and coworkers showed the formation of anodic porous oxides with ordered hole array structures by employing a pretexturing process for Cu, Zn and Ni[209]. However, the fabricated ordered nanohole arrays of $Cu_2O$, ZnO and NiO had limited thickness (less than 500 nm). The controllable fabrication of anodic films with highly ordered nanostructures on transition metals is still a major challenge. Although some formation mechanisms for nanostructured anodic films, especially nanoporous and nanotubular films, have been suggested, the nature of the nanostructure formation process is not very well understood and is still debated. In particular, the relationship between electrolyte systems and the morphologies of anodic films deserves further study. The understanding of formation mechanisms and continuous improvements in anodization techniques are crucial for the future of anodic films on transition metals. In short, the anodization field still holds many challenges and opportunities for researchers.

## DECLARATIONS

### Authors' contributions

Preparing the manuscript draft, writing-review, editing, funding acquisition: Jiang L
Writing-review: Li P, Wang S, van Ree T
Collecting literature: Liu R
Funding acquisition, supervision: Zhu X, Song Y

### Availability of data and materials
Not applicable.

### Financial support and sponsorship
This work was supported by the project from National Natural Science Foundation of China (Grant Nos. 51777097, 51577093).

### Conflicts of interest
All authors declares that there are no conflicts of interest.

### Ethical approval and consent to participate
Not applicable.

### Consent for publication
Not applicable.



## REFERENCES
1. Lee W, Park SJ. Porous anodic aluminum oxide: anodization and templated synthesis of functional nanostructures. *Chem Rev* 2014;114:7487-556. DOI PubMed
2. Masuda H, Fukuda K. Ordered metal nanohole arrays made by a two-step replication of honeycomb structures of anodic alumina. *Science* 1995;268:1466-8. DOI PubMed
3. Nielsch K, Choi JS, Schwirn K, Wehrspohn RB, Gösele U. Self-ordering regimes of porous alumina: The 10% porosity rule. *Nano Lett* 2002;2:677-80. DOI
4. Lee W, Schwirn K, Steinhart M, Pippel E, Scholz R, Gösele U. Structural engineering of nanoporous anodic aluminium oxide by pulse anodization of aluminium. *Nat Nanotech* 2008;3:234-9. DOI PubMed
5. Lee K, Tang Y, Ouyang M. Self-ordered, controlled structure nanoporous membranes using constant current anodization. *Nano Lett* 2008;8:4624-9. DOI PubMed
6. Gong D, Grimes CA, Varghese OK, et al. Titanium oxide nanotube arrays prepared by anodic oxidation. *J Mater Res* 2001;16:3331-4. DOI
7. Macak JM, Tsuchiya H, Taveira L, Aldabergerova S, Schmuki P. Smooth anodic $TiO_2$ nanotubes. *Angew Chem Int Ed* 2005;44:7463-5. DOI PubMed
8. Macak JM, Schmuki P. Anodic growth of self-organized anodic $TiO_2$ nanotubes in viscous electrolytes. *Electrochim Acta* 2006;52:1258-64. DOI
9. Albu SP, Ghicov A, Macak JM, Hahn R, Schmuki P. Self-organized, free-standing $TiO_2$ nanotube membrane for flow-through photocatalytic applications. *Nano Lett* 2007;7:1286-9. DOI PubMed
10. Lee K, Mazare A, Schmuki P. One-dimensional titanium dioxide nanomaterials: nanotubes. *Chem Rev* 2014;114:9385-454. DOI PubMed
11. Yang Y, Albu SP, Kim D, Schmuki P. Enabling the anodic growth of highly ordered $V_2O_5$ nanoporous/nanotubular structures. *Angew Chem Int Ed* 2011;50:9071-5. DOI PubMed
12. Yang Y, Lee K, Zobel M, et al. Formation of highly ordered $VO_2$ nanotubular/nanoporous layers and their supercooling effect in phase transitions. *Adv Mater* 2012;24:1571-5. DOI PubMed
13. Lee H, Kumbhar VS, Lee J, Choi Y, Lee K. Highly reversible crystal transformation of anodized porous $V_2O_5$ nanostructures for wide potential window high-performance supercapacitors. *Electrochim Acta* 2020;334:135618. DOI
14. Lee CY, Lee K, Schmuki P. Anodic formation of self-organized cobalt oxide nanoporous layers. *Angew Chem Int Ed* 2013;52:2077-81. DOI PubMed
15. Li Y, Wei B, Yu Z, et al. Bifunctional porous cobalt phosphide foam for high-current-density alkaline water electrolysis with 4000 h long stability. *ACS Sustainable Chem Eng* 2020;8:10193-200. DOI
16. Yang Y, Fei H, Ruan G, Xiang C, M J. Tour. Edge-oriented $MoS_2$ nanoporous films as flexible electrodes for hydrogen evolution reactions and supercapacitor devices. *Adv Mater* 2014;26:8163-8. DOI
17. Jin B, Zhou X, Huang L, Lickleder M, Yang M, Schmuki P. Aligned $MoO_x/MoS_2$ core-shell nanotubular structures with a high density of reactive sites based on self-ordered anodic molybdenum oxide nanotubes. *Angew Chem Int Ed* 2016;55:12252-56. DOI PubMed
18. Szkoda M, Trzciński K, Siuzdak K, Lisowska-Oleksiak A. Photocatalytical properties of maze-like $MoO_3$ microstructures prepared

by anodization of Mo plate. *Electrochim Acta* 2017;228:139-45. DOI

19. Jin B, Hejazi S, Chu H, et al. MoP-protected Mo oxide nanotube arrays for long-term stable supercapacitors. *Appl Mater Today* 2019;17:227-35. DOI
20. Yanagishita T, Masuda T, Kondo T, Masuda H. Highly ordered anodic porous oxides of transition metals fabricated by anodization combined with a pretexturing process. *Electrochem Commun* 2021;123:106916. DOI
21. Mor GK, Varghese OK, Paulose M, Shankar K, Grimes CA. A review on highly ordered, vertically oriented $TiO_2$ nanotube arrays: Fabrication, material properties, and solar energy applications. *Sol Energy Mater Sol Cells* 2006;90:2011-75. DOI
22. Regonini D, Bowen CR, Jaroenworaluck A, Stevens R. A review of growth mechanism, structure and crystallinity of anodized $TiO_2$ nanotubes. *Mat Sci Eng R* 2013;74:377-406. DOI
23. Riboni F, Nguyen NT, So S, Schmuki P. Aligned metal oxide nanotube arrays: key-aspects of anodic $TiO_2$ nanotube formation and properties. *Nanoscale Horiz* 2016;1:445-66. DOI PubMed
24. Prakasam HE, Varghese OK, Paulose M, Mor GK, Grimes CA. Synthesis and photoelectrochemical properties of nanopores iron (III) oxide by potentiostatic anodization. *Nanotechnology* 2006;17:4285-91. DOI
25. Song Y, Jiang L, Qi W, Lu C, Zhu X, Jia H. High-field anodization of aluminum in concentrated acid solutions and at higher temperatures. *J Electroanal Chem* 2012;673:24-31. DOI
26. Yang J, Huang H, Lin Q, et al. Morphology defects guided pore initiation during the formation of porous anodic alumina. *ACS Appl Mater Interfaces* 2014;6:2285-91. DOI PubMed
27. Albu SP, Ghicov A, Schmuki P. High aspect ratio, self-ordered iron oxide nanopores formed by anodization of Fe in ethylene glycol/$NH_4F$ electrolytes. *Phys Status Solidi RRL* 2009;3:64-6. DOI
28. Jagminas A, Mažeika K, Bernotas N, Klimas V, Selskis A, Baltrūnas D. Compositional and structural characterization of nanoporous films produced by iron anodizing in ethylene glycol solution. *Appl Surf Sci* 2011;257:3893-7. DOI
29. Habazaki H, Konno Y, Aoki Y, Skeldon P, Thompson GE. Galvanostatic growth of nanoporous anodic films on iron in ammonium fluoride-ethylene glycol electrolytes with different water contents. *J Phys Chem C* 2010;114:18853-9. DOI
30. Konno Y, Tsuji E, Skeldon P, Thompson GE, Habazaki H. Factors influencing the growth behaviour of nanoporous anodic films on iron under galvanostatic anodizing. *J Solid State Electrochem* 2012;16:3887-96. DOI
31. Santamaria M, Terracina S, Konno Y, Habazaki H, Di Quarto F. Physicochemical characterization and photoelectrochemical analysis of iron oxide films. *J Solid State Electrochem* 2013;17:3005-14. DOI
32. LaTempa TJ, Feng X, Paulose M, Grimes CA. Temperature-dependent growth of self-assembled hematite ($\alpha$-$Fe_2O_3$) nanotube arrays: rapid electrochemical synthesis and photoelectrochemical properties. *J Phys Chem C* 2009;113:16293-8. DOI
33. Rangaraju RR, Panday A, Raja KS, Misra M. Nanostructured anodic iron oxide film as photoanode for water oxidation. *J Phys D Appl Phys* 2009;42:135303. DOI
34. Rangaraju RR, Raja KS, Panday A, Misra M. An investigation on room temperature synthesis of vertically oriented arrays of iron oxide nanotubes by anodization of iron. *Electrochim Acta* 2010;55:785-93. DOI
35. Wu J, Liu L, Liu S, et al. High responsivity photoconductors based on iron pyrite nanowires using sulfurization of anodized iron oxide nanotubes. *Nano Lett* 2014;14:6002-9. DOI PubMed
36. Pawlik A, Hnida K, Socha RP, Wiercigroch E, Małek K, Sulka GD. Effects of anodizing conditions and annealing temperature on the morphology and crystalline structure of anodic oxide layers grown on iron. *Appl Surf Sci* 2017;426:1084-93. DOI
37. Lucas-Granados B, Sánchez-Tovar R, Fernández-Domene RM, García-Antón J. Controlled hydrodynamic conditions on the formation of iron oxide nanostructures synthesized by electrochemical anodization: effect of the electrode rotation speed. *Appl Surf Sci* 2017;392:503-13. DOI
38. Lucas-Granados B, Sánchez-Tovar R, Fernández-Domene RM, García-Antón J. Influence of electrolyte temperature on the synthesis of iron oxide nanostructures by electrochemical anodization for water splitting. *Int J Hydrogen Energ* 2018;43:7923-37. DOI
39. Lee CY, Wang L, Kado Y, Killian MS, Schmuki P. Anodic nanotubular/porous hematite photoanode for solar water splitting: substantial effect of iron substrate purity. *ChemSusChem* 2014;7:934-40. DOI PubMed
40. Mohapatra SK, John SE, Banerjee S, Misra M. Water photooxidation by smooth and ultrathin $\alpha$-$Fe_2O_3$ nanotube arrays. *Chem Mater* 2009;21:3048-55. DOI
41. Yu SH, Shin J, Kim JJ, Lee KJ, Sung YE. Vertically aligned iron oxide nanotube arrays and porous magnetite nanostructures as three-dimensional electrodes for lithium ion microbatteries. *RSC Adv* 2012;2:12177-81. DOI
42. Zhang Z, Hossain MF, Takahashi T. Fabrication of shape-controlled $\alpha$-$Fe_2O_3$ nanostructures by sonoelectrochemical anodization for visible light photocatalytic application. *Mater Lett* 2010;64:435-8. DOI
43. Zhang Z, Hossain MF, Takahashi T. Self-assembled hematite $\alpha$-$Fe_2O_3$ nanotube arrays for photoelectrocatalytic degradation of azo dye under simulated solar light irradiation. *Appl Catal B Environ* 2010;95:423-9. DOI
44. Jun H, Im B, Kim JY, et al. Photoelectrochemical water splitting over ordered honeycomb hematite electrodes stabilized by alumina shielding. *Energy Environ Sci* 2012;5:6375-82. DOI
45. Pervez SA, Kim D, Farooq U, et al. Crystalline iron oxide nanotube arrays with high aspect ratio as binder free anode for Li-ion batteries. *Phys Status Solidi A* 2014;211:1-6. DOI
46. Pervez SA, Kim D, Farooq U, et al. Comparative electrochemical analysis of crystalline and amorphous anodized iron oxide nanotube layers as negative electrode for LIB. *ACS Appl Mater Interfaces* 2014;6:11219-24. DOI PubMed
47. He J, Mao M, Lu Y, Jiang W, Liang B. Superhydrophobic anodized Fe surface modified with fluoroalkylsilane for application in

LiBr-water absorption refrigeration process. *Ind Eng Chem Res* 2017;56:495-504. DOI

48. Cheng H, Zheng L, Tsang CK, et al. Electrochemical fabrication and optical properties of periodically structured porous $Fe_2O_3$ films. *Electrochem Commun* 2012;2:178-81. DOI
49. Mushove T, Breault TM, Thompson LT. Synthesis and characterization of hematite nanotube arrays for photocatalysis. *Ind Eng Chem Res* 2015;54:4285-92. DOI
50. Xie K, Guo M, Huang H, Liu Y. Fabrication of iron oxide nanotube arrays by electrochemical anodization. *Corros Sci* 2014;88:66-75. DOI
51. Xie K, Li J, Lai Y, et al. Highly ordered iron oxide nanotube arrays as electrodes for electrochemical energy storage. *Electrochem Commun* 2011;13:657-60. DOI
52. Momeni MM, Ghayeb Y, Mohammadi F. $Fe_2O_3$ nanotube films prepared by anodisation as visible light photocatalytic. *Surf Eng* 2015;31:452-7. DOI
53. Rozana M, Razak KA, Yew CK, Lockman Z. Annealing temperature-dependent crystallinity and photocurrent response of anodic nanoporous iron oxide film. *J Mater Res* 2016;31:1681-90. DOI
54. Yang Y, Zhou J, Detsch R, et al. Biodegradable nanostructures: degradation process and biocompatibility of iron oxide nanostructured arrays. *Mat Sci Eng C* 2018;85:203-13. DOI PubMed
55. Xue Y, Jin W, Du H, Wang S, Zheng S, Zhang Y. Tuning a-$Fe_2O_3$ nanotube arrays for the oxygen reduction reaction in alkaline media. *RSC Adv* 2016;6:41878-84. DOI
56. Makimizu Y, Nguyen NT, Tucek J, et al. Activation of α-$Fe_2O_3$ for photoelectrochemical water splitting strongly enhanced by low temperature annealing in low oxygen containing ambient. *Chem Eur J* 2020;26:2685-92. DOI
57. Joseph JA, Nair SB, John KA, et al. Aluminium doping in iron oxide nanoporous structures to tailor material properties for photocatalytic applications. *J Appl Electrochem* 2020;50:81-92. DOI
58. Lucas-Granados B, Sánchez-Tovar R, Fernández-Domene RM, Estívalis-Martínez JM, García-Antón J. How does anodization time affect morphological and photocatalytic properties of iron oxide nanostructures? *J Mater Sci Technol* 2020;38:159-69. DOI
59. Martín-González M, Martinez-Moro R, Aguirre MH, Flores E, Caballero-Calero O. Unravelling nanoporous anodic iron oxide formation. *Electrochim Acta* 2020;330:135241. DOI
60. Syrek K, Kemona S, Czopor J, Zaraska L, Sulka GD. Photoelectrochemical properties of anodic iron oxide layers. *J Electroanal Chem* 2022;909:116143. DOI
61. Cao J, Gu Q, Gao N, et al. Designing micro-nano structure of anodized iron oxide films by metallographic adjustment on T8 steel. *Ceram Int* 2021;47:32954-62. DOI
62. Zhu X, Liu L, Song Y, et al. Oxygen bubble mould effect: serrated nanopore formation and porous alumina growth. *Monatsh Chem* 2008;139:999-1003. DOI
63. Zhu XF, Song Y, Liu L, et al. Electronic currents and the formation of nanopores in porous anodic alumina. *Nanotechnology* 2009;20:475303. DOI PubMed
64. Zhong XM, Yu DL, Zhang SY, et al. Fabrication and formation mechanism of triple-layered $TiO_2$ nanotubes. *J Electrochem Soc* 2013;160:125-9. DOI
65. Yu DL, Song Y, Zhu XF, Yang RQ. Han AJ. Morphological evolution of $TiO_2$ nanotube arrays with lotus-root-shaped nanostructure. *Appl Surf Sci* 2013;276:711-6. DOI
66. Li C, Ni Y, Gong J, Song Y, Gong T, Zhu X. A review: research progress on the formation mechanism of porous anodic oxides. *Nanoscale Adv* 2022;4:322-33. DOI PubMed PMC
67. Kang JS, Noh Y, Kim J, et al. Iron oxide photoelectrode with multidimensional architecture for highly efficient photoelectrochemical water splitting. *Angew Chem Int Ed* 2017;56:6583-8. DOI PubMed
68. Ali G, Park YJ, Hussain A, Cho SO. A novel route to the formation of 3D nanoflower-like hierarchical iron oxide nanostructure. *Nanotechnology* 2019;30:095601. DOI PubMed
69. Sagu JS, Wijayantha KGU, Bohm M, Bohm S, Rout TK. Anodized steel electrodes for supercapacitors. *ACS Appl Mater Interfaces* 2016;8:6277-85. DOI PubMed
70. Wang Q, Liu Q, Ni Y, Yang Y, Zhu X, Song Y. N-Doped $FeS_2$ achieved by thermal annealing of anodized Fe in ammonia and sulfur atmosphere: applications for supercapacitors. *J Electrochem Soc* 2021;168:080522. DOI
71. Wang H, Chen B, Zhang S, et al. Preparation and supercapacitive properties of 3D flower-like iron metaphosphates based on anodization of iron. *Thin Solid Films* 2022;742:139045. DOI
72. Makimizu Y, Yoo J, Poornajar M, et al. Effects of low oxygen annealing on the photoelectrochemical water splitting properties of α-$Fe_2O_3$. *J Mater Chem A* 2020;8:1315-25. DOI
73. Li Y, Cheng YF. Photocatalytic anti-bioadhesion and bacterial deactivation on nanostructured iron oxide films. *J Mater Chem B* 2018;6:1458-69. DOI PubMed
74. Murphy AB, Barnes PRF, Randeniya LK, et al. Efficiency of solar water splitting using semiconductor electrodes. *Int J Hydrogen Energy* 2006;31:1999-2017. DOI
75. Alexander BD, Kulesza PJ, Rutkowska I, Augustynski J. Metal oxide photoanodes for solar hydrogen production. *J Mater Chem* 2008;18:2298-303. DOI
76. Xue J, Zhang N, Shen Q, et al. In-situ construction of photoanode with $Fe_2O_3/Fe_3O_4$ heterojunction nanotube array to facilitate charge separation for efficient water splitting. *J Alloy Compd* 2022;918:165787. DOI

77. Joseph JA, Nair SB, John SS, Remillard SK, Shaji S, Philip RR. Zinc-doped iron oxide nanostructures for enhanced photocatalytic and antimicrobial applications. *J Appl Electrochem* 2021;51:521-38. DOI
78. Yu SH, Lee SH, Lee DJ, Sung YE, Hyeon T. Conversion reaction-based oxide nanomaterials for lithium ion battery anodes. *Small* 2016;12:2146-72. DOI PubMed
79. Zeng Y, Yu M, Meng Y, Fang P, Lu X, Tong Y. Iron-based supercapacitor electrodes: advances and challenges. *Adv Energy Mater* 2016;6:1601053. DOI
80. Li R, Gao N, Wang C, Ding G, Wang Y, Ma H. A facile strategy to in situ synthesize metal oxide/conductive polymer hybrid electrodes for supercapacitors. *Soft Matter* 2022;18:2517-21. DOI PubMed
81. Hickling A, Taylor D. The anodic behaviour of metals. part V-copper. *Trans Faraday Soc* 1948;44:262-8. DOI
82. Halliday JS. The anodic behaviour of copper in caustic soda solutions. *Trans Faraday Soc* 1954;50:171-8. DOI
83. Ashworth Y, Fairhurst D. The anodic formation of $Cu_2O$ in alkaline solutions. *J Electrochem Soc* 1977;124:506. DOI
84. Marchiano SL, Elsner CI, Arvia AJ. The anodic formation oxide films on copper and cathodic reduction of cuprous in sodium hydroxide solutions. *J Appl Electrochem* 1980;10:365-77. DOI
85. Daltin AL, Addad A, Chopart JP. Potentiostatic deposition and characterization of cuprous oxide films and nanowires. *J Cryst Growth* 2005;282:414-20. DOI
86. Lee YH, Leu IC, Wu MT, Yen JH, Fung KZ. Fabrication of Cu/$Cu_2O$ composite nanowire arrays on Si via AAO template-mediated electrodeposition. *J Alloy Compd* 2007;427:213-8. DOI
87. Shoesmith DW, Rummery TE, Owen D, Lee W. Anodic oxidation of copper in alkaline solutions I. nucleation and growth of cupric hydroxide films. *J Electrochem Soc* 1976;123:790-9. DOI
88. Wu X, Bai H, Zhang J, Chen F, Shi G. Copper hydroxide nanoneedle and nanotube arrays fabricated by anodization of copper. *J Phys Chem B* 2005;109:22836-42. DOI PubMed
89. Allam NK, Grimes CA. Electrochemical fabrication of complex copper oxide nanoarchitectures via copper anodization in aqueous and non-aqueous electrolytes. *Mater Lett* 2011;65:1949-55. DOI
90. Zhang Z, Wang P. Highly stable copper oxide composite as an effective photocathode for water splitting via a facile electrochemical synthesis strategy. *J Mater Chem* 2012;22:2456-64. DOI
91. Li Y, Chang S, Liu X, et al. Nanostructured CuO directly grown on copper foam and their supercapacitance performance. *Electrochim Acta* 2012;85:393-8. DOI
92. Hyam RS, Lee J, Cho E, Khim J, Lee H. Synthesis of copper hydroxide and oxide nanostructures via anodization technique for efficient photocatalytic application. *J Nanosci Nanotechnol* 2012;12:8396-400. DOI PubMed
93. Cheng Z, Du M, Fu K, Zhang N, Sun K. pH-controllable water permeation through a nanostructured copper mesh film. *ACS Appl Mater Interfaces* 2012;4:5826-32. DOI PubMed
94. Jiang W, He J, Xiao F, Yuan S, Lu H, Liang B. Preparation and antiscaling application of superhydrophobic anodized CuO nanowire surfaces. *Ind Eng Chem Res* 2015;54:6874-83. DOI
95. Xiao F, Yuan S, Liang B, Li G, Pehkonen SO, Zhang TJ. Superhydrophobic CuO nanoneedle-covered copper surfaces for anticorrosion. *J Mater Chem A* 2015;3:4374-88. DOI
96. Zhao J, Shu X, Wang Y, et al. Construction of CuO/$Cu_2O$@CoO core shell nanowire arrays for high-performance supercapacitors. *Surf Coat Tech* 2016;299:15-21. DOI
97. Stepniowski WJ, Stojadinović S, Vasilić R, et al. Morphology and photoluminescence of nanostructured oxides grown by copper passivation in aqueous potassium hydroxide solution. *Mater Lett* 2017;198:89-92. DOI
98. Wan J, Pang A, He D, Liu J, Suo H, Zhao C. A high-performance supercapacitor electrode based on three-dimensional poly-rowed copper hydroxide nanorods on copper foam. *J Mater Sci Mater Electron* 2018;29:2660-7. DOI
99. Du X, Xia C, Li Q, Wang X, Yang T, Yin F. Facile fabrication of $Cu_xO$ composite nanoarray on nanoporous copper as supercapacitor electrode. *Mater Lett* 2018;233:170-3. DOI
100. Wang B, Cao B, Wang C, Zhang Y, Yao H, Wang Y. The optical and electrical performance of CuO synthesized by anodic oxidation based on copper foam. *Materials* 2020;13:5411. DOI PubMed PMC
101. Zhang R, Chen C, Yu H, et al. All-solid-state wire-shaped asymmetric supercapacitor based on binder-free CuO nanowires on copper wire and PPy on carbon fiber electrodes. *J Electroanal Chem* 2021;893:115323. DOI
102. Song G, Liu S, Xia C, Song L, Yang T, Li Q. Synthesis and application of $Cu(OH)_2$ nanowires on nanoporous copper prepared by dealloying $Ti_{50}Cu_{50}$ and $Ti_{25}Zr_{25}Cu_{50}$ amorphous alloys. *Mater Charact* 2021:178;111258. DOI
103. Gong S, Liu X, Yue X, et al. Needle-like $Cu(OH)_2$ in situ grown on nanoporous copper ribbon via anodizing route for supercapacitors. *Mater Chem Phys* 2022;283:126046. DOI
104. Ghadge TS, Lokhande BJ. Post annealing temperature-dependent morphological and electrochemical properties of copper hydroxide thin film electrodes obtained by anodization of copper. *J Mater Sci* 2016;51:9879-88. DOI
105. He D, Wang G, Liu G, Suo H, Zhao C. Construction of leaf-like CuO-$Cu_2O$ nanocomposites on copper foam for high-performance supercapacitors. *Dalton Tran* 2017;46:3318-24. DOI PubMed
106. Anantharaj S, Sugime H, Noda S. Ultrafast growth of a $Cu(OH)_2$-CuO nanoneedle array on Cu foil for methanol oxidation electrocatalysis. *ACS Appl Mater Interfaces* 2020;12:27327-38. DOI PubMed
107. Anantharaj S, Sugime H, Yamaoka S, Noda S. Pushing the limits of rapid anodic growth of CuO/$Cu(OH)_2$ nanoneedles on cu for the methanol oxidation reaction: Anodization pH Is the game changer. *ACS Appl Energy Mater* 2021;4:899-912. DOI

108. Wang C, Cao J, Gao Z, Ji S, Ma H, Wang Y. Synthesizing robust cuprous oxide film with adjustable morphologies as surface-enhanced raman scattering substrate by copper anodization. *Mater Chem Phys* 2021;264:124470. DOI
109. Şişman O, Kılınç N, Öztürk ZZ. Structural, electrical and $H_2$ sensing properties of copper oxide nanowires on glass substrate by anodization. *Sensor Actuat B* 2016;236:1118-25. DOI
110. Jerez DPO, Teijelo ML, Cervantes WR, et al. Nanostructuring of anodic copper oxides in fluoride-containing ethylene glycol media. *J Electroanal Chem* ;807:181-6. DOI
111. Wang P, Ng YH, Amal R. Embedment of anodized p-type $Cu_2O$ thin films with CuO nanowires for improvement in photoelectrochemical stability. *Nanoscale* 2013;5:2952-8. DOI PubMed
112. Shu X, Zheng H, Xu G, et al. The anodization synthesis of copper oxide nanosheet arrays and their photoelectrochemical properties. *Appl Surf Sci* 2017;412:505-16. DOI
113. Shu X, Wang Y, Cui J, et al. Supercapacitive performance of single phase CuO nanosheet arrays with ultra-long cycling stability. *J Alloy Compd* 2018;753:731-9. DOI
114. Stępniowski WJ, Paliwoda D, Chen Z, Landskron K, Misiołek WZ. Hard anodization of copper in potassium carbonate aqueous solution. *Mater Lett* 2019;252:182-5. DOI
115. Stępniowski WJ, Misiołek WZ. The influence of electrolyte usage on the growth of nanostructured anodic films on copper in sodium carbonate aqueous solution. *J Electroanal Chem* 2020;857:113491. DOI
116. Abd-Elnaiem AM, Abdel-Rahim MA, Abdel-Latief AY, Mohamed AAR, Mojsilović K, Stępniowski WJ. Fabrication, characterization and photocatalytic activity of copper oxide nanowires formed by anodization of copper foams. *Materials* 2021;14:5030. DOI PubMed PMC
117. Stępniowski WJ, Paliwoda D, Abrahami ST, et al. Nanorods grown by copper anodizing in sodium carbonate. *J Electroanal Chem* 2020;857:113628. DOI
118. Stępniowski WJ, Wang KK, Chandrasekar S, Paliwoda D, Nowak-Stępniowska A, Misiołek WZ. The impact of ethylenediaminetetraacetic acid (EDTA) additive on anodization of copper in $KHCO_3$ - hindering $Cu^{2+}$ re-deposition by EDTA influences morphology and composition of the nanostructures. *J Electroanal Chem* 2020;871:114245. DOI
119. Babu TGS, Ramachandran T. Development of highly sensitive non-enzymatic sensor for the selective determination of glucose and fabrication of a working model. *Electrochim Acta* 2010;55:1612-8. DOI
120. Huang HY, Chien DJ, Huang GG, Chen PY. Electrochemical preparation of photoelectrochemically active CuI thin films from room temperature ionic liquid. *Electrochim Acta* 2012;65:204-9. DOI
121. Vishwanath RS, Kandaiah S. Electrochemical preparation of crystalline γ-CuI thin films through potential-controlled anodization of copper and its photoelectrochemical investigations. *J Solid State Electr* 2016;20:2093-102. DOI
122. Zhou C, Cheng J, Hou K, Zhu Z, Zheng Y. Preparation of $CuWO_4$@$Cu_2O$ film on copper mesh by anodization for oil/water separation and aqueous pollutant degradation. *Chem Eng J* 2017;307:803-11. DOI
123. Hu H, Wang X, Gong L, Yu X, Yang X, Zhao J. Preparation of leaflike copper phosphate films by anodic oxidation and their catalytic oxidation performance. *Catal Commun* 2017;95:46-9. DOI
124. Antonopoulos IA, Karantonis A. Electrochemistry of copper in methanolic solutions: anodic oxidation and fabrication of hydrophobic surfaces. *Electrochim Acta* 2017;240:195-202. DOI
125. Lu Y, Liu X, Qiu K, et al. Facile synthesis of graphene-like copper oxide nanofilms with enhanced electrochemical and photocatalytic properties in energy and environmental applications. *ACS Appl Mater Interfaces* 2015;7:9682-90. DOI PubMed
126. Liu S, Wang J, Pei X, et al. The reversible wetting transition between superhydrophilicity and superhydrophobicity of tremella-like CuxO@CuxS nanosheets prepared by one-step anodization and the application of on-demand oil/water separation. *J Alloy Compd* 2021;889:161793. DOI
127. Meng M, Li R, Zuo L, Luo X, Zhang T. Fabrication of hierarchical porous metallic glasses decorated with Cu nanoparticles as integrated electrodes for high-performance non-enzymatic glucose sensing. *Scripta Mater* 2021;199:113884. DOI
128. Sisman O, Kilinc N, Akkus UO, et al. Hybrid liquid crystalline zinc phthalocyanine@$Cu_2O$ nanowires for $NO_2$ sensor application. *Sens Actuators B Chem* 2021;345:130431. DOI
129. Yamamoto R, Kowalski D, Zhu R, et al. Fabrication of superhydrophobic copper metal nanowire surfaces with high thermal conductivity. *Appl Surf Sci* 2021;537:147854. DOI
130. Paracchino A, Laporte V, Sivula K, Grätzel M, Thimsen E. Highly active oxide photocathode for photoelectrochemical water reduction. *Nature Mater* 2011;10:456-61. DOI PubMed
131. Joya KS, de Groot HJM. Controlled surface-assembly of nanoscale leaf-type Cu-oxide electrocatalyst for high activity water oxidation. *ACS Catal* 2016;6:1768-71. DOI
132. Zhang Z, Zhong C, Liu L, Teng X, Wu Y, Hu W. Electrochemically prepared cuprous oxide film for photo-catalytic oxygen evolution from water oxidation under visible light. *Sol Energy Mater Sol Cells* 2015;132:275-81. DOI
133. Majumdar D, Ghosh S. Recent advancements of copper oxide based nanomaterials for supercapacitor applications. *J Energy Storage* 2021;34:101995. DOI
134. Chen J, Xu J, Zhou S, Zhao N, Wong CP. Facile and scalable fabrication of three-dimensional $Cu(OH)_2$ nanoporous nanorods for solid-state supercapacitors. *J Mater Chem A* 2015;3:17385-91. DOI
135. Huber K. Anodic formation of coatings on magnesium, zinc, and cadmium. *J Electrochem Soc* 1953; 100:376-82. DOI
136. Dirkse TP. Electrolytic oxidation of zinc in alkaline solutions. *J Electrochem Soc* 1955; 102:497-501. DOI

137. Fry H, Whitaker M. The anodic oxidation of zinc and a method of altering the characteristics of the anodic films. *J Electrochem Soc* 1959;106:606-11. DOI
138. Bockris JO, Nagy Z, Damjanovic A. On the deposition and dissolution of zinc in alkaline solutions. *J Electrochem Soc* 1972;119:285-95. DOI
139. Szpak S, Gabriel CJ. The Zn-KOH system: the solution-precipitation path for anodic ZnO formation. *J Electrochem Soc* 1979;126:1914-23. DOI
140. El Ela AH, Bahay ME, El-Raghy SM. Anodic oxidation and self-polarization of zinc metal. *J Mater Sci* 1981;16:2726-36. DOI
141. Liu MB, Cook GM, Yao NP. Passivation of zinc anodes in KOH electrolytes *J Electrochem Soc* 1981;128:1663-8. DOI
142. Nanto H, Minami T, Takata S. Intense white photoluminescence in ZnO thin film formed by anodization. *J Mater Sci* 1983;18:2721-6. DOI
143. Yamaguchi Y, Yamazaki M, Yoshihara S, Shirakashi T. Photocatalytic ZnO films prepared by anodizing. *J Electroanal Chem* 1998;442:1-3. DOI
144. Wu X, Lu G, Li C, Shi G. Room-temperature fabrication of highly oriented ZnO nanoneedle arrays by anodization of zinc foil. *Nanotechnology* 2006;17:4936-40. DOI
145. Sreekantan S, Gee LR, Lockman Z. Room temperature anodic deposition and shape control of one-dimensional nanostructured zinc oxide. *J Alloy Compd* 2009;476:513-18. DOI
146. Huang GS, Wu XL, Cheng YC, Shen JC, Huang AP, Chu PK. Fabrication and characterization of anodic ZnO nanoparticles. *Appl Phys A* 2007;86:463-7. DOI
147. Masuda R, Kowalski D, Kitano S, Aoki Y, Nozawa T, Habazaki H. Characterization of dark-colored nanoporous anodic films on zinc. *Coatings* 2020;10:1014. DOI
148. Hu Z, Chen Q, Li Z, Yu Y, Peng LM. Large-scale and rapid synthesis of ultralong ZnO nanowire films via anodization. *J Phys Chem C* 2010;114:881-9. DOI
149. Kim YT, Park J, Kim S, Park DW, Choi J. Fabrication of hierarchical ZnO nanostructures for dye-sensitized solar cells. *Electrochim Acta* 2012;78:417-21. DOI
150. Park J, Kim K, Choi J. Formation of ZnO nanowires during short durations of potentiostatic and galvanostatic anodization. *Curr Appl Phys* 2013;13:1370-5. DOI
151. Samir N, Eissa DS, Allam NK. Self-assembled growth of vertically aligned ZnO nanorods for light sensing applications. *Mater Lett* 2014;137:45-8. DOI
152. Yavaş A, Güler S, Erol M. Growth of ZnO nanoflowers: effects of anodization time and substrate roughness on structural, morphological, and wetting properties. *J Aust Ceram Soc* 2020;56:995-1003. DOI
153. Tantray AM, Shah MA. Photo electrochemical ability of dense and aligned ZnO nanowire arrays fabricated through electrochemical anodization. *Chem Phys Lett* 2020;747:137346. DOI
154. Tantray AM, Mir JF, Mir MA, Rather J, Shah MA. Random oriented ZnO nanorods fabricated through anodization of zinc in $KHCO_3$ electrolyte. *ECS J Solid State Sci* 2021;10:081003. DOI
155. Miles DO, Cameron PJ, Mattia D. Hierarchical 3D ZnO nanowire structures via fast anodization of zinc. *J Mater Chem A* 2015;3:17569-77. DOI
156. Mah CF, Beh KP, Yam FK, Hassan Z. Rapid formation and evolution of anodized-Zn nanostructures in $NaHCO_3$ solution. *ESC J Solid State Sci Technol* 2016;5:M105-12. DOI
157. Zaraska L, Mika K, Syrek K, Sulka GD. Formation of ZnO nanowires during anodic oxidation of zinc in bicarbonate electrolytes. *J Electroanal Chem* 2017;801:511-20. DOI
158. Zaraska L, Mika K, Hnida KE, et al. High aspect-ratio semiconducting ZnO nanowires formed by anodic oxidation of Zn foil and thermal treatment. *Mater Sci Eng B* 2017;226:94-8. DOI
159. Zamora-Peredo L, Ceballos-Valle A, Báez-Rodríguez A, Hernández-Torres J, García- González L, Orozco-Cruz R. Raman spectroscopy of ZnO nanowires obtained by electrochemical anodization: effect of thermal treatment, voltage and anodizing time. *ECS Trans* 2019;94:329-37. DOI
160. Tantray AM, Shah MA. Photo electrochemical stability response of ZnO nanoflowers fabricated through single step electrochemical anodization. *Chem Pap* 2021;75:1739-47. DOI
161. Lee W, Ji R, Gösele U, Nielsch K. Fast fabrication of long-range ordered porous alumina membranes by hard anodization. *Nat Mater* 2006;5:741-7. DOI PubMed
162. Chu SZ, Wada K, Inoue S, Isogai M, Yasumori A. Fabrication of ideally ordered nanoporous alumina films and integrated alumina nanotubule arrays by high-field anodization. *Adv Mater* 2005;17:2115-9. DOI
163. Huang W, Yu M, Cao S, Wu L, Shen X, Song Y. Fabrication of highly ordered porous anodic alumina films in 0.75 M oxalic acid solution without using nanoimprinting. *Mater Res Bull* 2019;111:24-33. DOI
164. Kim SJ, Lee J, Choi J. Understanding of anodization of zinc in an electrolyte containing fluoride ions. *Electrochim Acta* 2008;53:7941-45. DOI
165. Tello A, Boulett A, Sánchez J, et al. An unexplored strategy for synthesis of ZnO nanowire films by electrochemical anodization using an organic-based electrolyte. Morphological and optical properties characterization. *Chem Phys Lett* 2021;778:138825. DOI
166. Katwal G, Paulose M, Rusakova IA, Martinez JE, Varghese OK. Rapid growth of zinc oxide nanotube−nanowire hybrid architectures and their use in breast cancer-related volatile organics detection. *Nano Lett* 2016;16:3014-21. DOI PubMed

167. Dong H, Zhou J, Virtanen S. Fabrication of ZnO nanotube layer on Zn and evaluation of corrosion behavior and bioactivity in view of biodegradable applications. *Appl Surf Sci* 2019;494:259-65. DOI
168. Batista-Grau P, Sánchez-Tovar R, Fernández-Domene RM, García-Antón J. Formation of ZnO nanowires by anodization under hydrodynamic conditions for photoelectrochemical water splitting. *Surf Coat Tech* 2020;381:125197. DOI
169. Batista-Grau P, Fernández-Domene RM, Sánchez-Tovar R, García-Antón J. Control on the morphology and photoelectrocatalytic properties of ZnO nanostructures by simple anodization varying electrolyte composition. *J Electroanal Chem* 2021;880:114933. DOI
170. Shrestha NK, Lee K, Hahn R, Schmuki P. Anodic growth of hierarchically structured nanotubular ZnO architectures on zinc surfaces using a sulfide based electrolyte. *Electrochem Commun* 2013;34:9-13. DOI
171. Sanz-Marco A, Sánchez-Tovar R, Bajo MM, Fernández-Domene RM, García-Antón J. Cathodoluminescence characterization of ZnO/ZnS nanostructures anodized under hydrodynamic conditions. *Electrochim Acta* 2018;269:553-9. DOI
172. Aydın EB. Electrochemical synthesize and characterization of ZnO/ZnS nanostructures for hydrogen production. *Int J Energy Res* 2020;44:1-16. DOI
173. Basu PK, Bhattacharyya P, Saha N, Saha H, Basu S. The superior performance of the electrochemically grown ZnO thin films as methane sensor. *Sensor Actuat B* 2008;133:357-63. DOI
174. Basu PK, Bontempi E, Maji S, Saha H, Basu S. Variation of optical band gap in anodically grown nanocrystalline ZnO thin films at room temperature-effect of electrolyte concentrations. *J Mater Sci Mater Electron* 2009;20:1203-7. DOI
175. Shetty A, Nanda KK. Synthesis of zinc oxide porous structures by anodization with water as an electrolyte. *Appl Phys A* 2012;109:151-7. DOI
176. Voon CH, Tukiman N. T, Lim BY, et al. Synthesis of zinc oxide thin film by anodizing. In 2014 IEEE International Conference on Semiconductor Electronics, 2014. p. 420-3. DOI
177. Ono S, Kobayashi Y, Asoh H. Self-organized and high aspect ratio nanoporous zinc oxide prepared by anodization. *ECS Trans* 2008;13:183-9. DOI
178. Dong J, Liu Z, Dong J, et al. Self-organized ZnO nanorods prepared by anodization of zinc in NaOH electrolyte. *RSC Adv* 2016;6:72968-74. DOI
179. Mika K, Socha RP, Nyga P, et al. Electrochemical synthesis and characterization of dark nanoporous zinc oxide films. *Electrochim Acta* 2019;305:349-59. DOI
180. Shrestha NK, Hahn R, Lee K, Tighineanu A, Schmuki P. Electrochemically assisted self-assembling of $ZnF_2$-ZnO nanospheres: formation of hierarchical thin porous films. *ECS Electrochem Lett* 2014;3:E1-E3. DOI
181. Diomidis N, Celis JP. Effect of hydrodynamics on zinc anodizing in silicate-based electrolytes. *Surf Coat Technol* 2005;195:307-13. DOI
182. Kim SJ, Choi J. Self-assembled arrays of ZnO stripes by anodization. *Electrochem Commun* 2008;10:175-9. DOI
183. He S, Zheng M, Yao L, et al. Preparation and properties of ZnO nanostructures by electrochemical anodization method. *Appl Surf Sci* 2010;256:2557-62. DOI
184. Zhao J, Wang X, Liu J, Meng Y, Xu X, Tang C. Controllable growth of zinc oxide nanosheets and sunflower structures by anodization method. *Mater Chem Phys* 2011;126:555-9. DOI
185. Zhao J, Wang X, Sun Y, Liu J, Tang C. Preparation and formation mechanism of microporous spheric zinc phosphate. *J Solid State Electrochem* 2011;15:1861-5. DOI
186. Farrukh MA, Thong CK, Adnan R, Kamarulzaman MA. Preparation and characterization of zinc oxide nanoflakes using anodization method and their photodegradation activity on methylene blue. *Russ J Phys Chem A* 2012;86:2041-8. DOI
187. Heo B, Kim YT, Choi J. Electrochemical synthesis of zinc ricinoleate and its application in ammonia adsorption. *J Environ Chem Eng* 2021;9:105083. DOI
188. Pearton SJ, Norton DP, Ip K, Heo YW, Steiner T. Recent progress in processing and properties of ZnO. *Prog Mater Sci* 2005;50:293-340. DOI
189. Chang SS, Yoon SO, Park HJ, Sakai A. Luminescence properties of anodically etched porous Zn. *Appl Surf Sci* 2000;158:330-4. DOI
190. Yang J, Liu G, Lu J, Qiu Y, Yang S. Electrochemical route to the synthesis of ultrathin ZnO nanorod/nanobelt arrays on zinc substrate. *Appl Phys Lett* 2007;90:103109. DOI
191. Galstyan V, Comini E, Baratto C, Faglia G, Sberveglieri G. Nanostructured ZnO chemical gas sensors. *Ceram Int* 2015;41:14239-44. DOI
192. Gilani S, Ghorbanpour M, Jadid AP. Antibacterial activity of ZnO films prepared by anodizing. *J Nanostruct Chem* 2016;6:183-9. DOI
193. Ramirez-Canon A, Miles DO, Cameron PJ, Mattia D. Zinc oxide nanostructured films produced via anodization: a rational design approach. *RSC Adv* 2013;3:25323-30. DOI
194. Ramirez-Canon A, Medina-Llamas M, Vezzoli M, Mattia D. Multiscale design of ZnO nanostructured photocatalysts. *Phys Chem Chem Phys* 2018;20:6648-56. DOI PubMed
195. Taylor CM, Ramirez-Canon A, Wenk J, Mattia D. Enhancing the photo-corrosion resistance of ZnO nanowire photocatalysts. *J Hazard Mater* 2019;378:120799. DOI PubMed
196. Ozdemir ET, Kartal U, Dikici T, Erol M, Yurddaskal M. A comparative study on structural, morphological and photocatalytic properties of anodically grown ZnO nanowires under varying parameters. *J Mater Sci Mater Electron* 2021;32:27398-408. DOI

197. Batista-Grau P, Fernández-Domene RM, Sánchez-Tovar R, Blasco-Tamarit E, Solsona B, García-Antón J. Indirect charge transfer of holes via surface states in ZnO nanowires for photoelectrocatalytic applications. *Ceram Int* 2022;48:21856-67. DOI
198. Zhu E, Li F, Zhao Q, et al. Preparation, parameter optimization of anodized ZnO films and their photocatalytic performance in organic dye degradation in wastewater. *Appl Phys A* 2022;128:697. DOI
199. Huang MC, Wang TH, Wu BJ, Lin JC, Wu CC. Anodized ZnO nanostructures for photoelectrochemical water splitting. *Appl Surf Sci* 2016;360:442-50. DOI
200. Mika K, Syrek K, Uchacz T, Sulka GD, Zaraska L. Dark nanostructured ZnO films formed by anodic oxidation as photoanodes in photoelectrochemical water splitting. *Electrochim Acta* 2022;414:140176. DOI
201. Chang H, Wu YR, Han X, Yi TF. Recent developments in advanced anode materials for lithium-ion batteries. *Energy Mater* 2021;1:100003. DOI
202. Chen X, Liu J, Yuan T, et al. Recent advances in earth-abundant first-row transition metal (Fe, Co and Ni)-based electrocatalysts for the oxygen evolution reaction. *Energy Mater* 2022;2:200028. DOI
203. Feng S, Tang Y, Xiao T. Anodization, precursor route to flowerlike patterns composed of nanoporous tin oxide nanostrips on tin substrate. *J Phys Chem C* 2009;113:4809-13. DOI
204. Lee JW, Park SJ, Choi WS, Shin HC. Well-defined meso- to macro-porous film of tin oxides formed by an anodization process. *Electrochim Acta* 2011;56:5919-25. DOI
205. Wang M, Yang H, Liu Y. Current oscillations during potentiostatic anodization of tin in alkaline electrolytes. *Electrochim Acta* 2011;56:7051-7. DOI
206. Bian H, Tian Y, Lee C, Yuen MF, Zhang W, Li YY. Mesoporous $SnO_2$ nanostructures of ultrahigh surface areas by novel anodization. *ACS Appl Mater Interfaces* 2016;8:28862-71. DOI PubMed
207. Li P, Niu D, He M, et al. Growth model of the tin anodizing process and the capacitive performance of porous tin oxides. *J Phys Chem C* 2020;124:3050-58. DOI
208. Gao N, Cao J, Wang C, et al. Study on the crystallinity and oxidation states of nanoporous anodized tin oxide films regulated by annealing treatment for supercapacitor application. *Langmuir* 2022;38:164-73. DOI PubMed
209. Yanagishita T, Masuda T, Masuda H. Preparation of ordered nanohole array structures by anodization of prepatterned Cu, Zn, and Ni. *RSC Adv* 2022;12:6848-54. DOI PubMed PMC